FOSSIL ENERGY

DOE/MT/94011-10
(OSTI ID: 805233)

STUDY OF THE EFFECTS OF AMBIENT CONDITIONS UPON THE PERFORMANCE OF FAN POWERED, INFRARED, NATURAL GAS BURNERS

Final Report
November 1997

Date Published: December 2002

Work Performed Under Contract No. DE-FG22-94MT94011

Clark Atlanta University
Atlanta, Georgia

National Energy Technology Laboratory
National Petroleum Technology Office
U.S. DEPARTMENT OF ENERGY
Tulsa, Oklahoma

DOE/MT/94011-10
Distribution Category UC-122

Study of the Effects of Ambient Conditions Upon the Performance of Fan Powered, Infrared, Natural Gas Burners

December 2002

Work Performed Under DE-FG22-94MT94011

Prepared for
U.S. Department of Energy
Assistant Secretary for Fossil Energy

John Ford, Project Manager
National Energy Technology Laboratory
National Petroleum Technology Office
One West Third Street, Suite 1400
Tulsa, OK 74103

Prepared by
Department of Engineering
Clark Atlanta University
Atlanta, Georgia 30314

AGAR Research
8501 East Pleasant Valley Road
Cleveland, Ohio 44131

Energy International, Inc.
127 Bellevue Way SE, Suite 200
Bellevue, Washington 98004-6229

TABLE OF CONTENTS

page

LIST OF FIGURES

LIST OF TABLES

Energy International/AGAR Report No. A9762022

STUDY OF THE EFFECTS OF AMBIENT CONDITIONS UPON THE PERFORMANCE OF FAN POWERED, INFRARED, NATURAL GAS BURNERS

INTRODUCTION

This final report describes work performed under DOE Grant No. DE-FG22-94MT94011 during the period September 1, 1994 to May 28, 1997. The objective of this investigation is to characterize the operation of a fan-powered, infrared burner (IR burner) at various gas compositions and ambient conditions, develop numerical model to simulate the burner performances, and provide design guidelines for appliances containing PIR burners for satisfactory performance.

The fan-powered, infrared burner is a technology introduced more recently in the residential and commercial markets. It is a surface combustor that elevates the temperature of the burner head to a radiant condition. A variety of metallic and ceramic materials are used for the burner heads. It has been demonstrated that infrared burners produce low CO and NO_x emissions in a controlled geometric space [1]. As the environmental regulations become more stringent, infrared burners are receiving increasing interests.

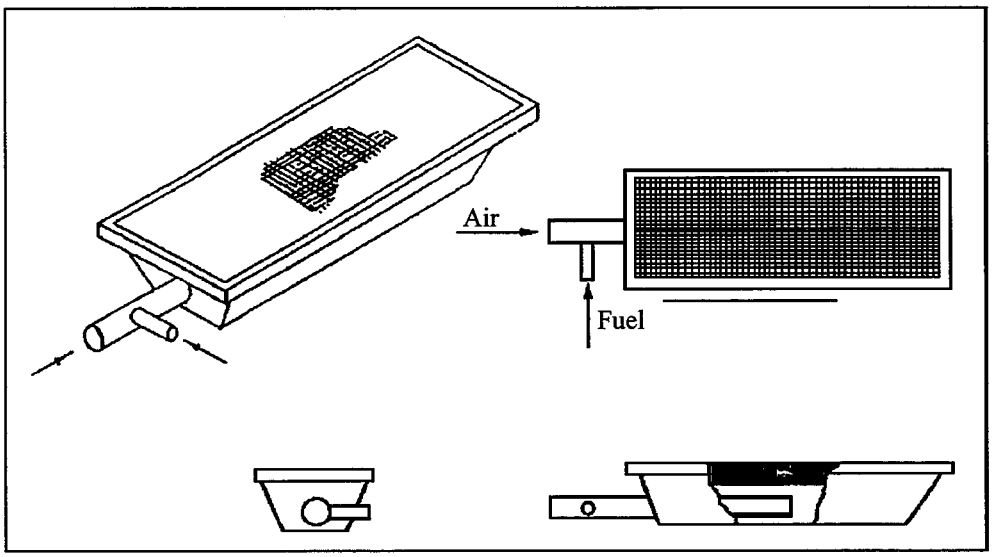

Figure 1. A Schematic of the Infrared Burner

The burner tested in this project is installed in a deep fat fryer. It consists of a pressurized air supply, an air/fuel mixing chamber, and a porous ceramic radiant tile (see **Figure 1**). Combustion takes place on the surface of the perforated ceramic tile creating a radiant heat source. One main reason for the present interest in this type of burner is its low NO_x emissions. This is attributed to the fact that a large proportion of the heat of combustion

is given out as radiation from the burner surface. This results in relatively low gas temperature in the combustion zone compared to that of a conventional free-flame burner. Applications of radiant burners include boilers, air heaters, deep fat fryers, process heaters, and immersion heaters.

The performance of natural gas-fired heating and cooking equipment is strongly dependent on ambient conditions and natural gas composition. In the United States, ambient temperature, pressure, and relative humidity vary significantly by location and season [2]. Also, natural gas compositions supplied by local gas distribution companies exhibit seasonal and regional variations [2]. These variations can cause reliability and performance problems in gas-fired equipment. In service, IR burners have had reliability and performance problems, especially when exposed to various gas compositions, operating altitudes, and other ambient conditions like temperature and humidity[3]. These parameters also affect the composition of the gaseous emissions from these burners. Burning characteristics will differ in important respects, one of the most important being speed of flame propagation that significantly affects the flame stability of the burner. It is the responsibility of the manufacturers to design appliances capable of performing more satisfactorily under reasonably wide variations in gas composition while retaining desirable efficiencies and operation.

There have been limited studies of the effects of gas composition upon the performance of radiant burners [2][3][4]. Due to the lack of data and fundamental understandings, the IR burner product development in the industry is empirical in nature and is conducted with one gas composition. This project characterizes the operation of IR burner at various gas compositions and ambient conditions and develops a baseline numerical analysis model to predict the behavior of these burners to the change in fuel compositions and other factors.

EXPERIMENTAL PROCEDURES

To conduct the experiments, an infrared combustor experimental setup has been developed and installed in the Combustion Laboratory at Clark Atlanta University (see **Figure 2**). This setup consists of a commercial deep fat fryer that has been modified to allow in-situ radiation measurements on the surface of the infrared burner via a view port installed on the side wall of the oil vat. The fuel/air flow rates were set and monitored by mass flow controllers. Exhaust gas emission measurement was conducted using a system consisting of six stand-alone gas analyzers which include CO, CO_2, O_2, NO_x, SO_x, and Unburned Total Hydrocarbons analyzers. These commercial gas analyzers (Horiba Instruments Inc., Irvine, CA), their sample conditioning units, and a lab-made sampling manifold were used to collect exhaust gases for CO, CO_2, O_2, NO_x and total unburned hydrocarbon (UHC) analyses. The gas analyzer was calibrated with gases of known composition. The exhaust gas sample was continuously taken through a ¼-inch stainless steel tube from the exhaust of the burner. The opening of the sampling tube was placed about five inch deep into the exhaust chimney. A gas pump was connected to the sampling tube to convert the traditional vacuum-gas-sampling system for the gas analyzer to a positive-pressure-gas-sampling system, which prevented the air leakage into the sample line and increased the measurement accuracy. Three measurements were made for each test condition, and their average was used for the final calculation and discussion. The relative standard deviations of three measurements for all the

experiments were less than 1%. During the emission measurement, the view port for the IR measurement were completely sealed to avoid air leakage into the combustion zone.

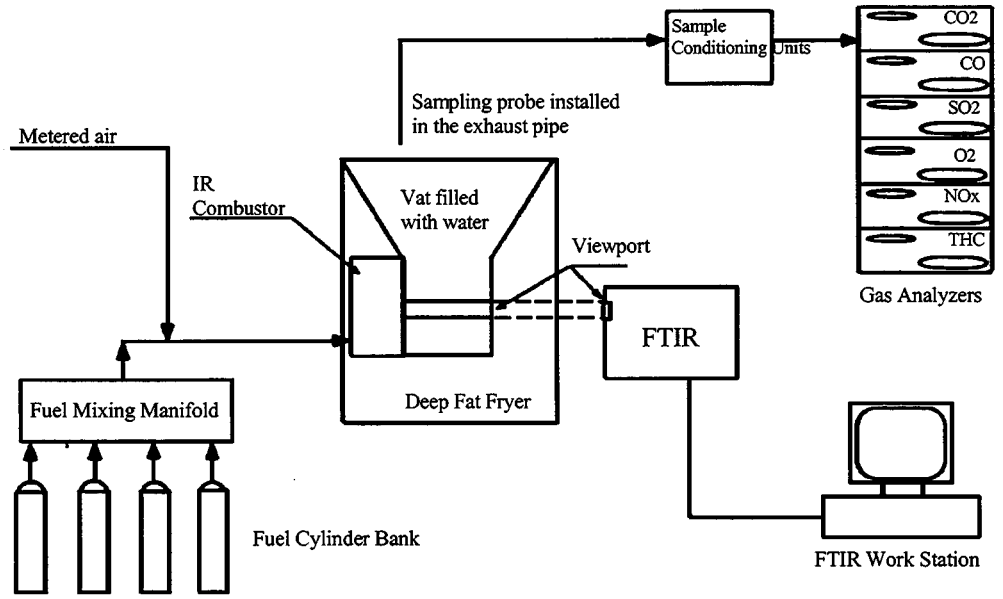

Figure 2. A Schematic of the Experimental Set-up

Since accurate IR radiation measurement is critical in the experimental study of the radiant burner's performance, various instrumentation to measure the radiant output from the infrared burner has been evaluated. In the developed experimental setup, an FTIR, System 2000 from Perkin Elmer (Perkin-Elmer Co., Norwalk, CT) is used for in-situ measurements of the radiant output from the surface of the burner. This spectroscopy system consists of a 15798.01 cm^{-1} reference laser, an external source and an internal (temperature stabilized wire coil) source options, a 12.50 mm Jacquinot-stop aperture with the resolution of 6.48 cm^{-1}, an interferometer with a beamsplitter of 6500 - 450 cm^{-1}, and an air-cooled triglycine sulfate detector (TGS, 15600 - 200 cm^{-1}). The TGS detector has a better background contribution compared to other kinds of detectors, which is important for the wide-band radiation measurement. Perkin-Elmer Spectrum for Windows version 1.0 software was used for spectral manipulation. All radiation measurements were conducted by using the burner as the external source. The effective aperture window size for the external source and the distance between the external source and instrumental interferometer were precisely controlled in the same conditions for all of the measurements. To reduce the fluctuation of test results, four scans were added and averaged for each spectra with a nominal resolution of 8 cm^{-1} in the range of 6500 - 450 cm^{-1}. Before the radiation measurements, the instrument was usually warmed up for more than two hours and, by design, it automatically tuned up (aligned) for the maximum sensitivity. Then a background spectrum from room-temperature-air was taken. The radiation-measurement spectral manipulation such as baseline correction and subtraction were made from the background measurement. Since the radiant signals were very strong, (the measurement noises were relatively small), the spectra were used for the total radiant energy calculation without further noise reduction and smoothing. The FTIR spectroscopy

was calibrated for the radiant energy calculation by using a Graseby Infrared 564 blackbody (Graseby Co. Orlando, Florida). The detailed calibration process is described as follows:

The infrared spectrum from a commercial deep fat fryer, shown in **Figure 3**, covers the IR range from 6,500 to 450 cm^{-1} and concentrates its spectral intensity in the 4,000 to 500 cm^{-1} wavenumber range with strong H_2O absorbances at 2,000 - 1,400 and 3,700 - 3,650 cm^{-1}, and CO_2 absorbances at about 2,350, 2,330 and 667 cm^{-1} [5]-[7], respectively. The measured spectrum is used to calculate the total radiant energy from the burner, as shown in **Figure 4**, since the radiant energy is proportional to the integration of the measured spectrum within the wavenumber range.

To quantify the radiant energy out through the measured spectrum, a blackbody has been used to calibrate the FTIR. A blackbody absorbs all of the radiant energy emitted to it. Moreover, the radiant energy emitted by a blackbody depends on its temperature alone. Therefore, the radiant energy emitted from the blackbody can be controlled precisely by simply controlling its temperature.

The Graseby Infrared blackbody used for the calibration has a typical infrared spectrum, as shown in **Figure 5**. It is very similar to that from a gas burner (see **Figure 3**), which also covers the infrared range of 6,500 - 450 cm^{-1} and has the strong intensity distribution between 4,000 and 500 cm^{-1}. When plotting the two spectra together, they are well overlapped with each other, except for the CO_2 absorbance peak, as shown in **Figure 6**. This is because the blackbody was heated by electricity. The CO_2 absorbance from the blackbody's spectrum was caused by the atmospheric CO_2, which was only about 0.04% by volume. On the other hand, the gas burner was heated by burning fuel in air, where up to 12% of CO_2 could be present. Calibration has been carried out in which the blackbody's temperature was increased step by step, and the spectrum at each temperature was measured and integrated to obtain the total area under the spectrum. This integrated magnitudes of the blackbody spectra from 6,500 to 450 cm^{-1} were then compared with the known total radiant energy output from the blackbody, which was calculated from its operating temperature. As expected the integrated area proportionally increased as the blackbody's temperature increased (see **Figure 7**). A fourth-order-polynomial equation between the integrated area and the blackbody's temperature were obtained through regression:

$$a = 2418.7 - 38.51\,T + 0.2075\,T^2 - 2.825 \times 10^{-4}\,T^3 + 1.583 \times 10^{-7}\,T^4 \quad (1)$$

where a is the integrated area of the infrared spectra from 6500 to 450 cm^{-1}, T is the temperature in °C, and the regression coefficient is $R^2 = 0.9984$.

On the other hand, the radiant energy (or emissive power) $E_{b,\lambda}(\lambda,T)$ of a blackbody at a given wavelength λ and absolute temperature T is given by Planck's law [10] as

$$E_{b,\lambda}(\lambda,T) = C_1 / \{\lambda^5 (e^{C2/\lambda t} - 1)\} \quad (2)$$

The total radiant energy $E_b(T)$ of the blackbody is the radiation emitted by it at all wavelengths. Mathematically, it is expressed as the Stefan-Boltzmann law [11]:

$$E_b(T) = \int_0^\infty E_{b,\lambda}(\lambda,T)\, d\lambda = \delta\, T^4 \quad (3)$$

Where, δ is the Stefan-Boltzmann constant given by

$$\delta = (\pi/C_2)^4 C_1/15 \qquad (4)$$

where $C_1 = 3.743 \times 10^8$ W-μm^4/m^2, and $C_2 = 1.4387 \times 10^4$ μm K. By combining Eqs. 3 and 4, we have

$$E_b(T) = 5.685 \times 10^{-8} T^4 \qquad (5)$$

where $E_b(T)$ is in W/m^2 and T is in K. Eq. 5 is the result of the Stefan-Boltzmann law integrated for wavelength from 0 to ∝ (or wavenumber from ∝ to 0). Since the result in **Figure 5** shows that most of the radiant energy from the infrared burner is located in the range of 4,000 to 500 cm^{-1}, it is reasonable to assume the spectrum from this wavenumber range can effectively represent the total radiant energy with negligible error. Therefore, by using Eq. 5, the total radiant energy, $E_b(T)$, from the blackbody is plotted against its temperature in **Figure 6**, where the units for the E_b and T have been converted into W/cm^2 and °C, respectively. Since both Eqs. 1 and 5 are fourth order, the curve in **Figure 8** is similar to that in **Figure 7**.

By combining the data in **Figures 7** and **8**, the total radiation energy, $E_b(T)$, is plotted against the integrated infrared energy magnitude in **Figure 9**, which shows a very-well-fitted straight line with regression equation as

$$E_b(T) = -0.06391 + 2.975 \times 10^{-4} a \qquad (6)$$

where *a* is the IR magnitude integrated from 6,500 to 450 cm^{-1}, the regression coefficient is $R^2 = 0.9921$.

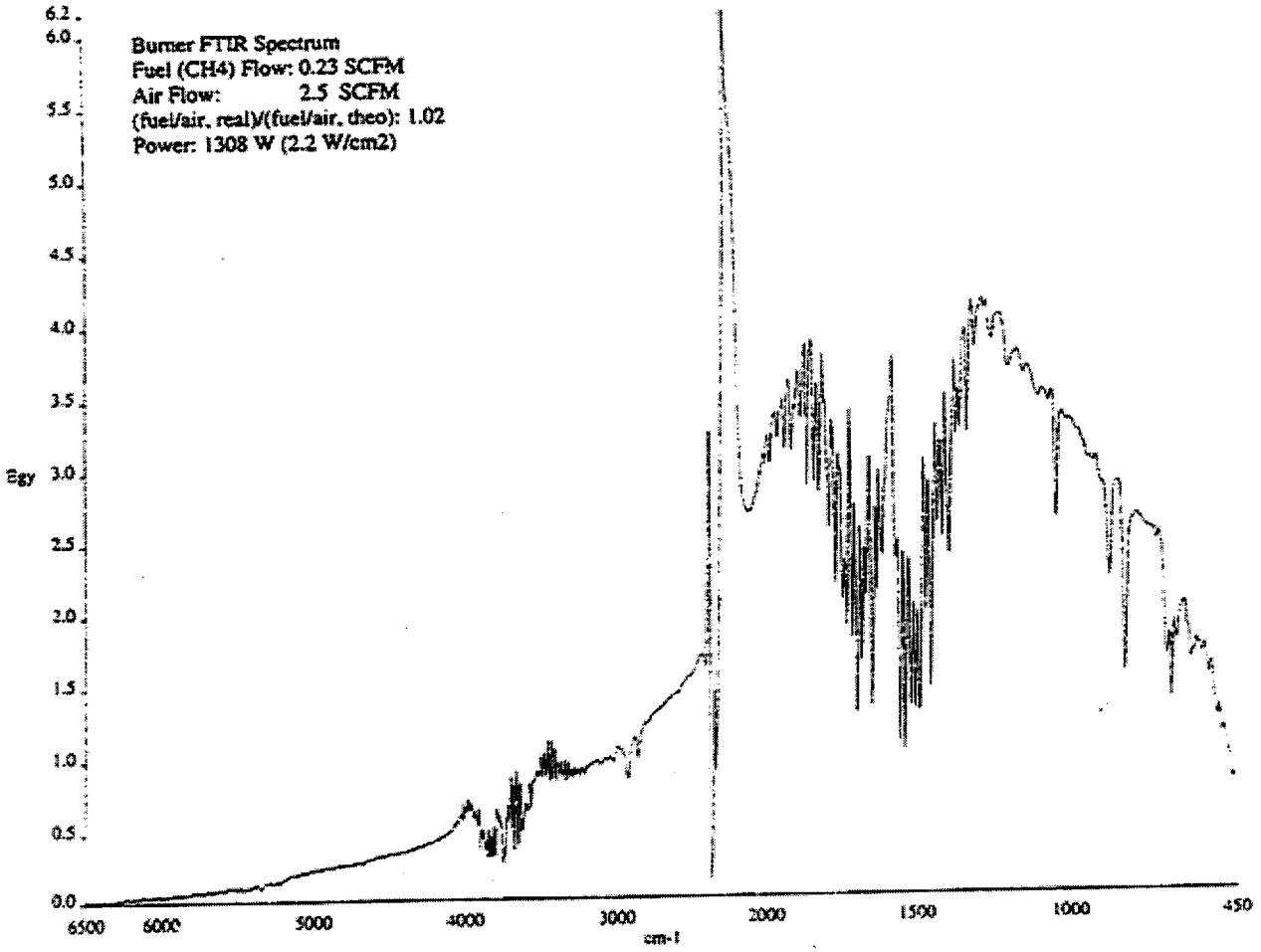

Figure 3. FTIR Spectrum of the Infrared Burner

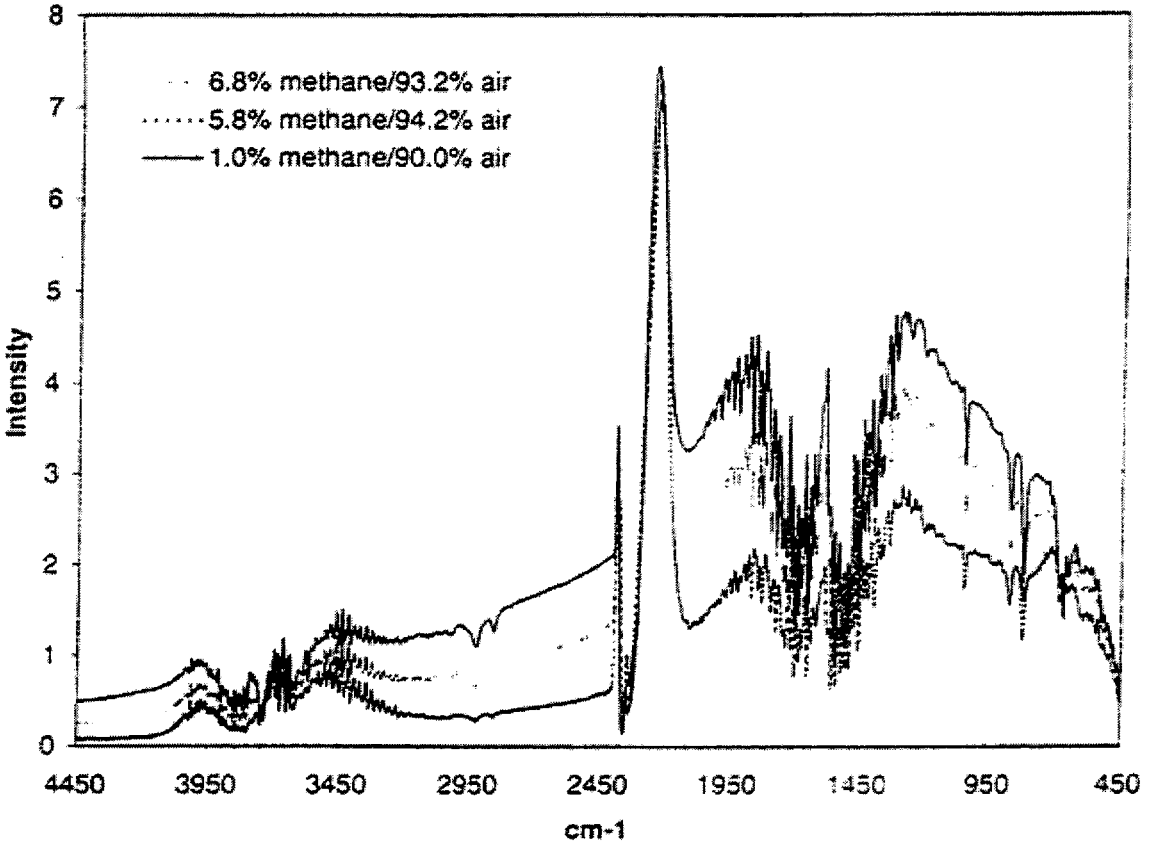

Figure 4. **FTIR Spectrum of the Infrared Burner at Different Methane/Air Ratios**

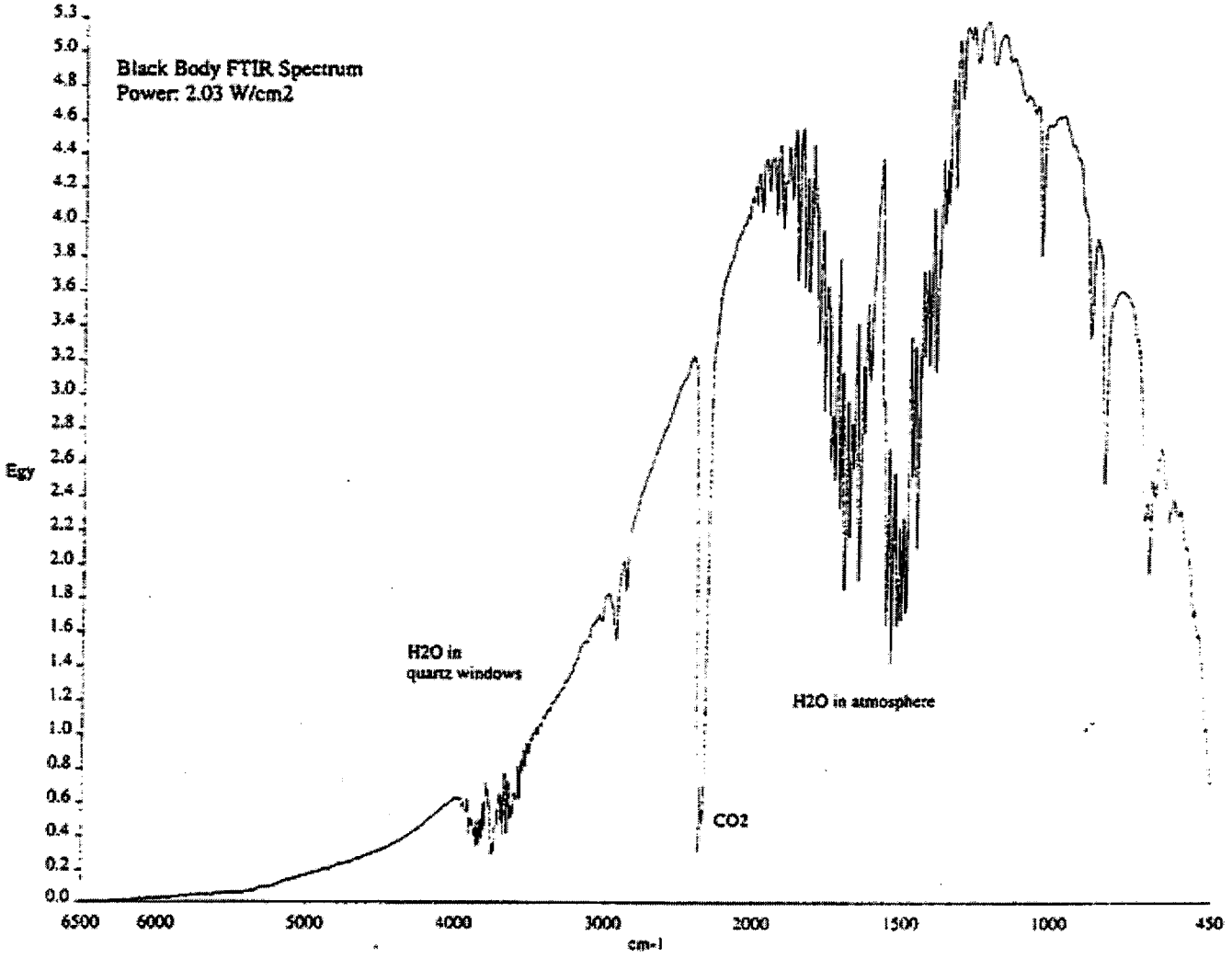

Figure 5. FTIR Spectrum of the Black Body

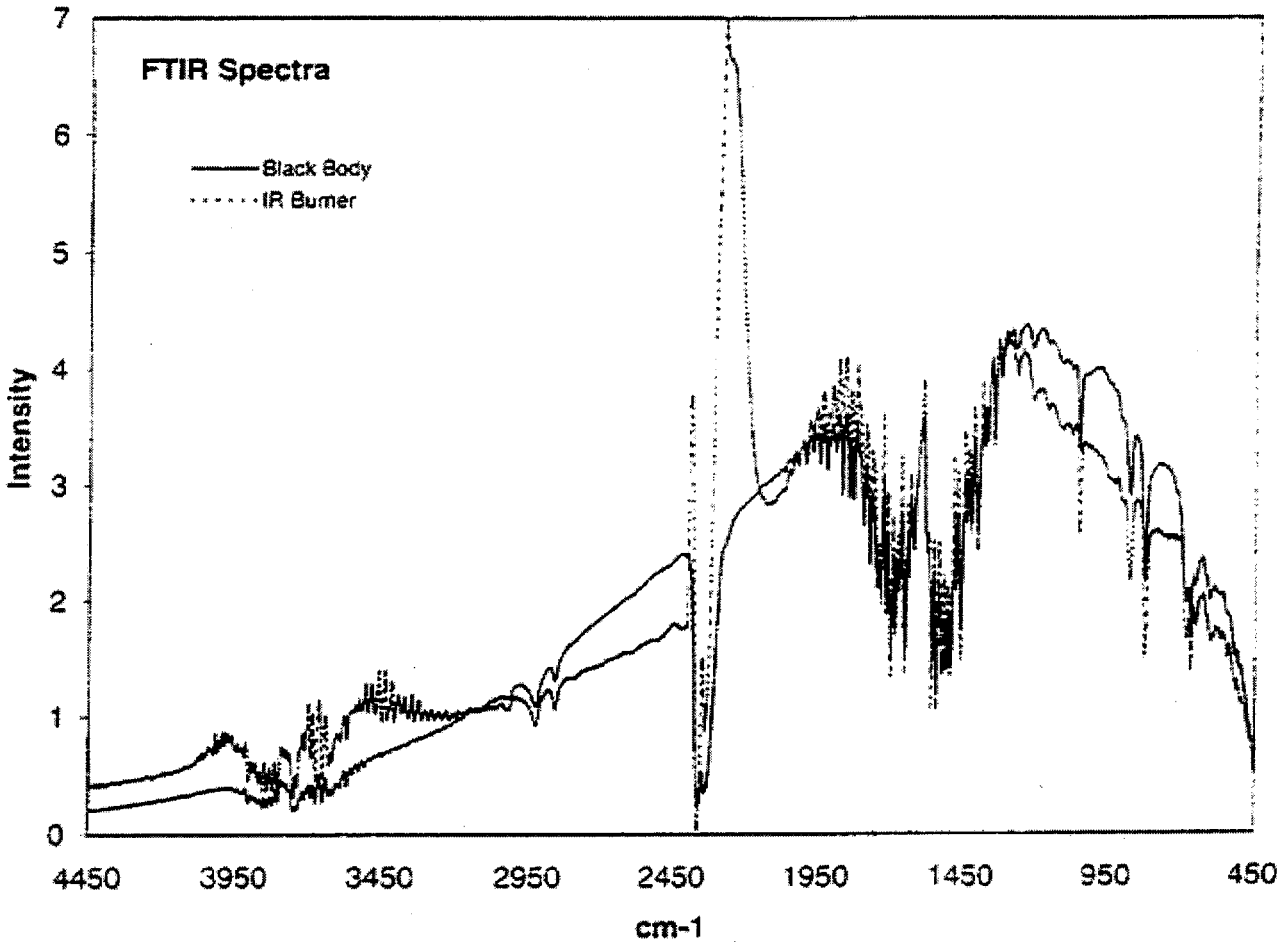

Figure 6. FTIR Spectra of the Infrared Burner and the Black Body

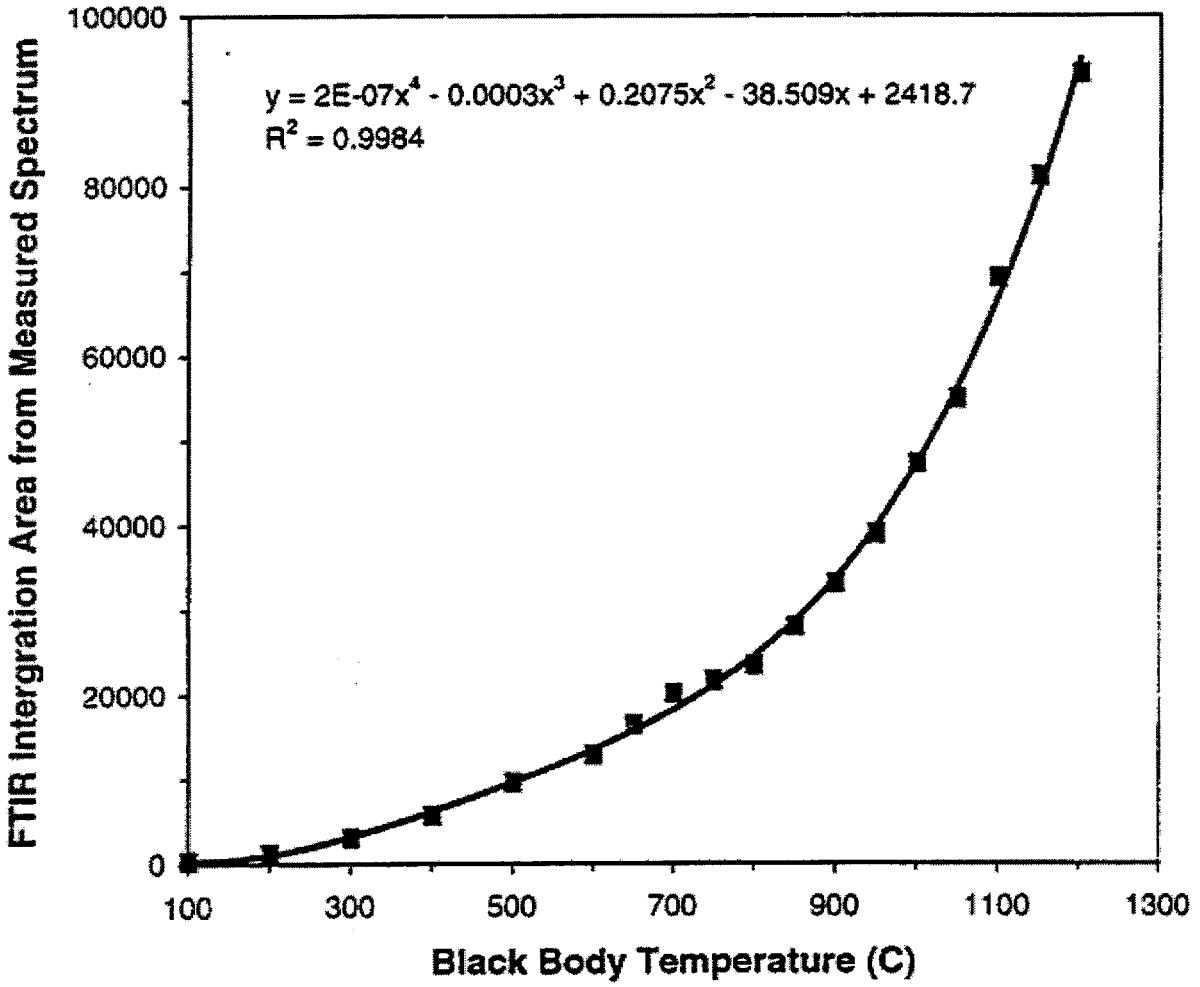

Figure 7. **Relationship Between the Measured FTIR Integration Area (6,500 - 450 cm^{-1}) and the Blackbody Temperature (°C)**

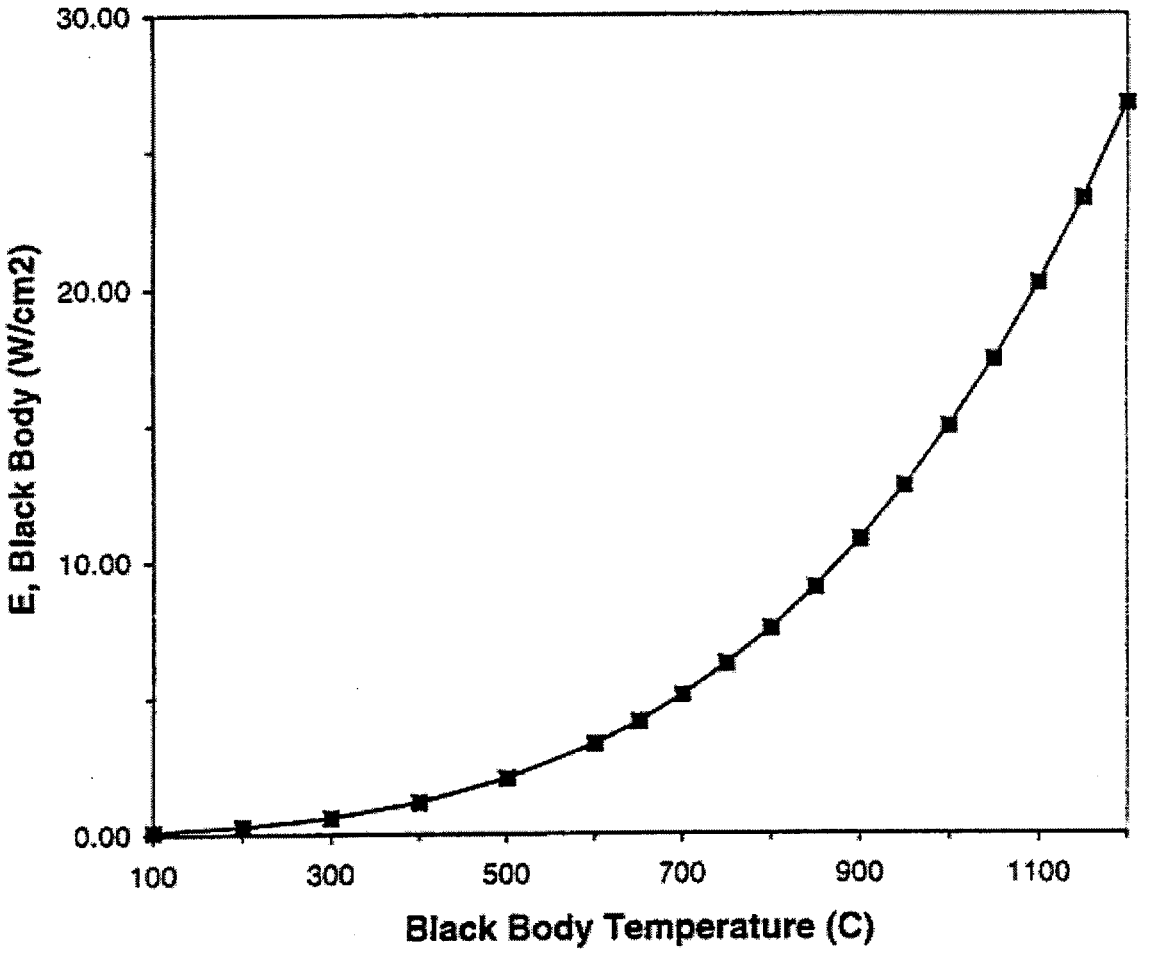

Figure 8. **Relationship Between the Total Radiant Energy ($E_b(T)$) Calculated from the Stefan-Boltzmann Law and the Blackbody Temperature (°C)**

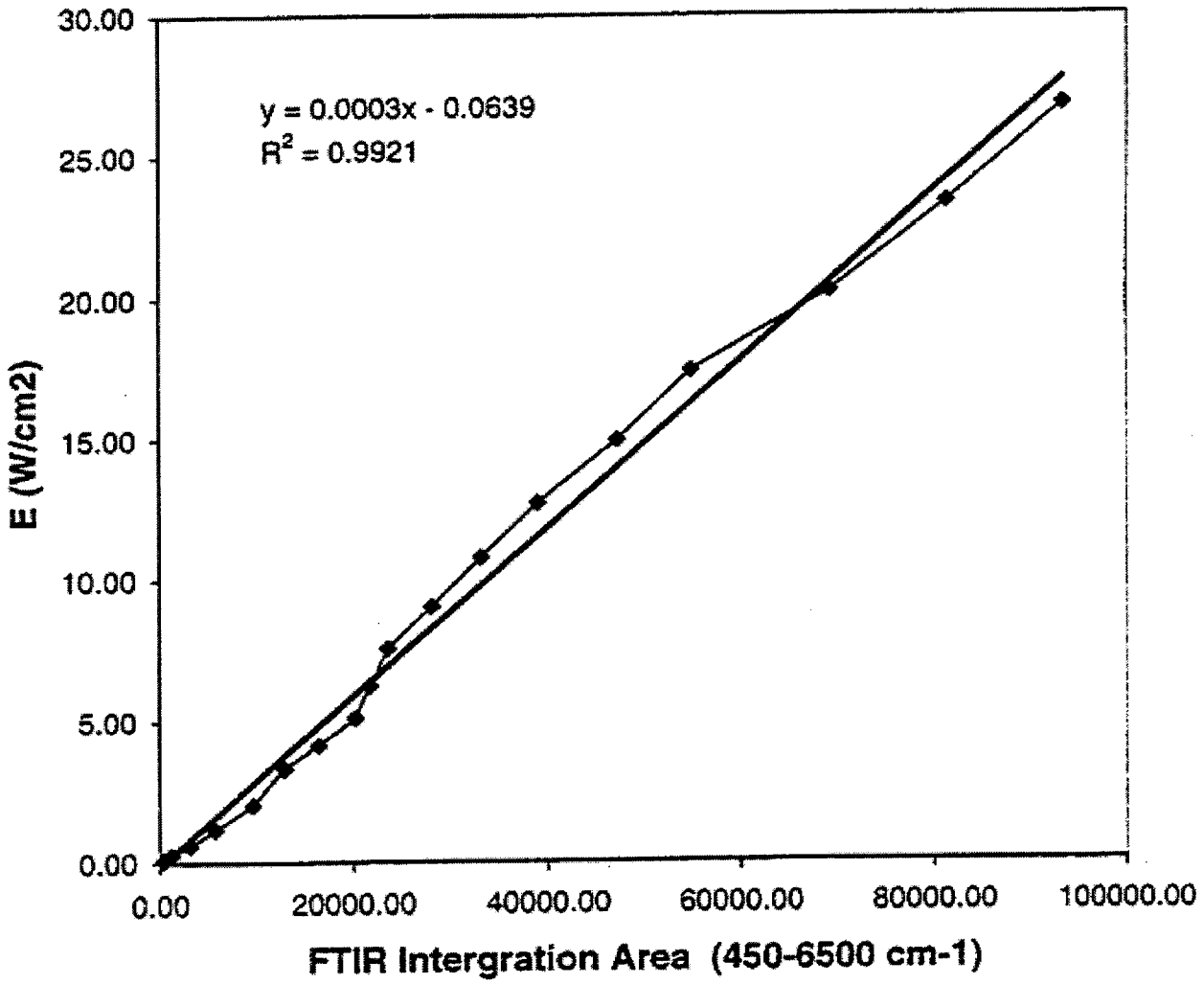

Figure 9. **Relationship Between the Total Radiant Energy ($E_b(T)$) Calculated from the Stefan-Boltzmann Law and the measured FTIR Integration Area (6,500 - 450 cm^{-1})**

EXPERIMENTAL RESULTS

Experiments have been conducted for an extensive test matrix of fuel gas mixtures that represent the complete range of gas compositions usually encountered in the United States. Instrumentation grade methane was used as the baseline fuel. Mixtures of methane/propane and methane/hydrogen are used to study the effect of fuel mixtures on the performance of the radiant burners. The performance of the burner is investigated in terms of its radiant efficiency (ratio of radiative flux generated by the burner to the total energy input by fuel) and gaseous emissions at various gas compositions and air/fuel ratios. Tests results have been reported in previous project quarterly technical progress reports. Major findings are briefly summarized as follows:

Radiant Energy Measurement

All the radiant energies were calculated from the measured and corrected infrared data by using Eq. 6. The radiant efficiency was defined as the ratio of the calculated radiant energy to the combustion enthalpy (energy) of the input fuels.

A typical result of radiation energy measurement is shown in **Figure 10**, which shows the radiant efficiency at different equivalence ratio Φ. The equivalence ration is defined as the ratio of the actual fuel-air ratio to the theoretical fuel-air ratio. It can be seen that in the fuel-lean combustion region as the equivalence ratio increased from 0.55 to 0.95, the radiant efficiency increased steadily. At $\Phi = 1$, where the stoichiometric fuel-air ratio for combustion was reached, the radiant efficiency reached its maximum, ~31.4%. After that point, the combustion took place in the fuel-rich combustion region. As Φ was further increased, the radiant efficiency decreased, due to the reduced burner surface temperature. Due to the need of open access to the burner surface for the radiation measurement, the view port of was open when the radiation measurement was conducted. This inevitably introduced some uncertainty in the combustion air flow rate measurement. Typically, results show that the maximum radiant efficiency of the combustor occurred in a range where $0.95 < \Phi < 1$. In order to determine the effect caused by the air leakage through the open view port, a glass window was used to seal the open view port, and the measurement was made by passing the infrared radiation through the glass window. Since glass had strong absorbances in some IR bands, the measured absolute spectral magnitudes were distorted and much smaller in magnitude. However, these measurement showed that radiant efficiency always reached its maximum at $\Phi = 1$.

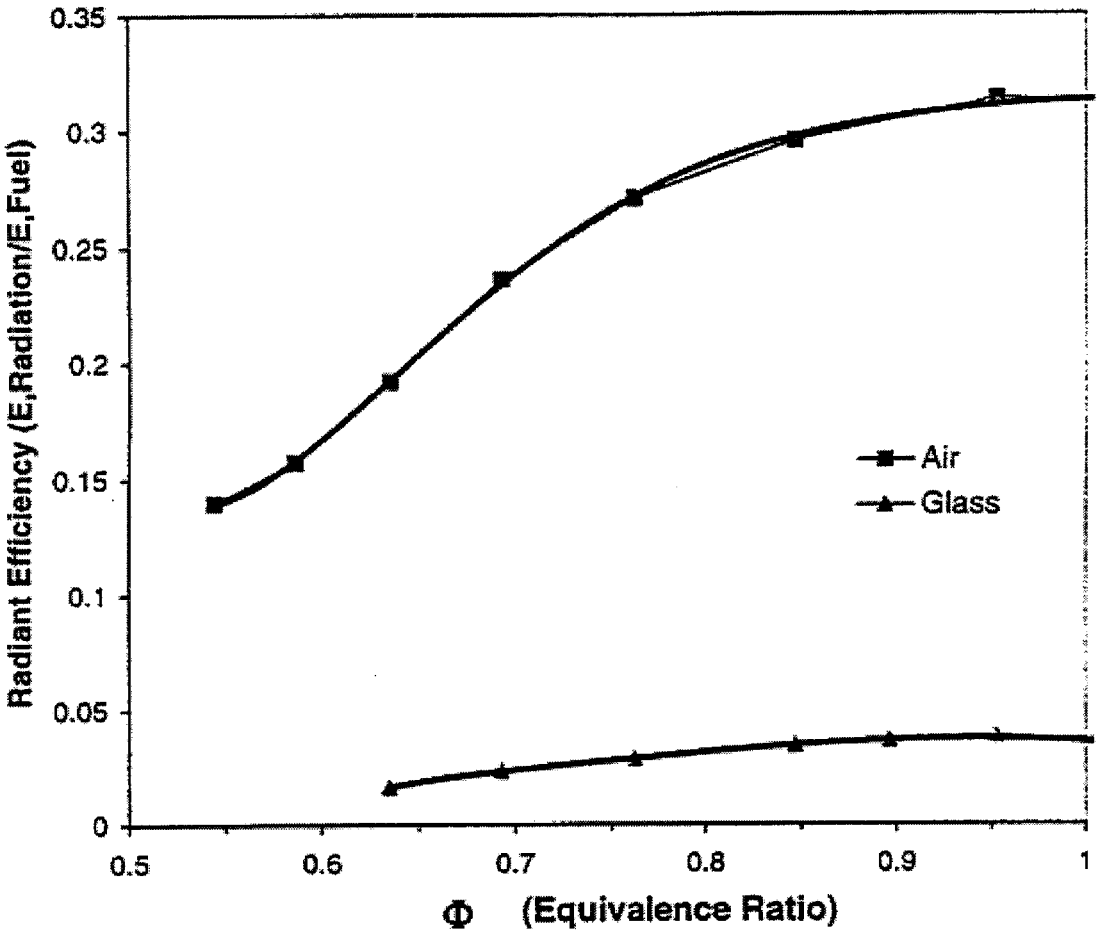

Figure 10. **Relationship of the Radiant Efficiency (the measured radiant energy / the total input fuel energy) and the Equivalence Ratio (the actual fuel-air ratio / the theoretical fuel-air ratio) for the Methane-Air Combustion**

Effect of Nitrogen Addition on Radiant Efficiency

Nitrogen was added into the fuel flow to study the flamelift and assess the combustor performance. Typical results are shown in **Figure 11**. It shows that as nitrogen was added to the methane-air mixture before combustion the radiant efficiency was decreased, and the maximum efficiency region was shifted to the fuel-rich range. The reduction of radiant efficiency is believed to be caused by the gas dilution. Since nitrogen is a non-combustible gas, it absorbs the combustion energy and reduced the ceramic tile temperature. As a result, the radiant energy output was reduced. As 2.4% and 7% of nitrogen (based on the amount of methane) were added to the methane-air mixture, the radiant efficiency of combustion were decreased by about 1% and 3%, respectively. It is interesting to note that in the fuel-lean combustion region the nitrogen-dilution effects were greater, which resulted in the maximum efficiency shifted to the fuel-rich combustion region as shown in **Figure 11.**

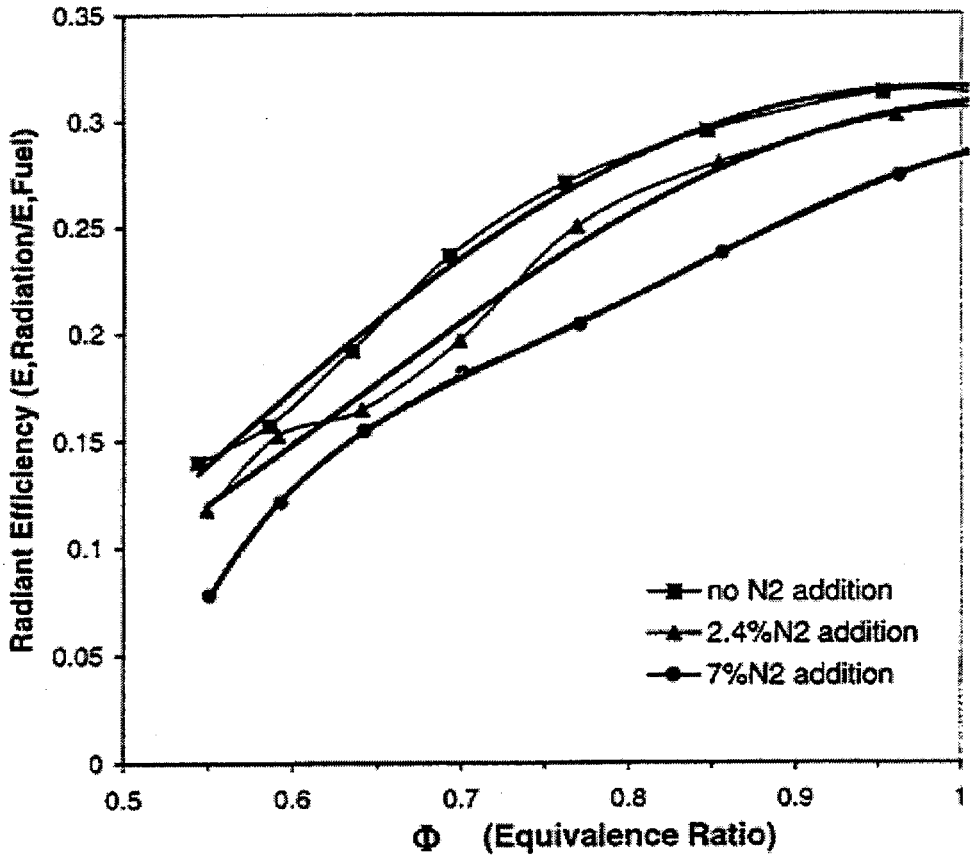

Figure 11. Effects of the N_2 Addition on the Radiant Efficiency

Effect of Propane Addition on Radiant Efficiency

Propane is added into methane to simulate the gas compositions when distribution and pipeline companies inject propane into pipeline gases to meet the peak demand. Usually propane is introduced in the main gas stream while maintaining acceptable values for heating value and specific gravity. Typical practice is up to 20% of the overall volume at peak use. This change of gas composition will result in changes in equivalence ratio, which has an impact on combustor performance, efficiency, and emissions. In addition, adding propane in the fuel provided an opportunity to study the effect of sooting on the performance of the combustor.

Typical results when propane was added into the fuel are shown in **Figure 12**. The results in this figure indicate that the addition of propane to the methane did not affect much of the radiant efficiency of the combustion, at least in the fuel-lean combustion region. This may be because propane and methane have quite similar physical and chemical properties. Both propane and methane are straight-chain saturated hydrocarbons at the gaseous state in the ambient temperature and pressure. They also produce the same combustion products, CO_2, and water, as shown in Eqs. 7 and 8.

$$CH_4 + 2\,O_2 = CO_2 + 2\,H_2O \qquad (7)$$

$$C_3H_8 + 5\,O_2 = 3\,CO_2 + 4\,H_2O \qquad (8)$$

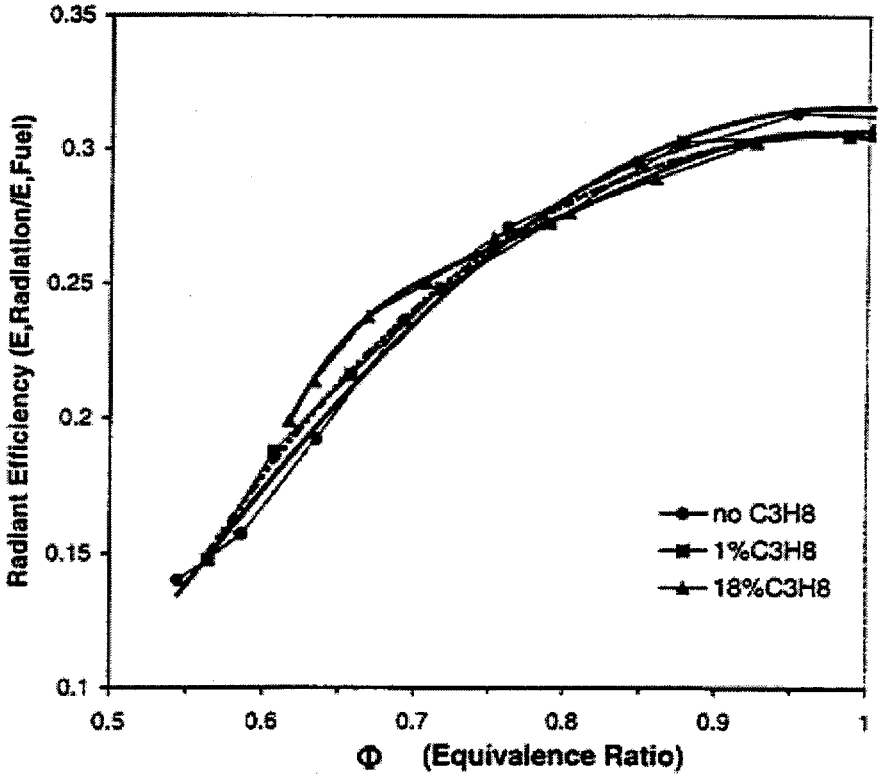

Figure 12. Effects of the Propane (C_3H_8) Addition on the Radiant Efficiency

When completely combusted in the air, the exhaust produced from one mole methane consists of N_2 = 2 × 79/21 = 7.52 moles, CO_2 = 1 mole, and H_2O = 2 moles. The heat capacities of N_2, CO_2, and H_2O are 29.1, 37.1, and 33.6 J/mole K, respectively [8]. So the total exhaust gas heat capacity from one mole methane combustion is 7.52 × 29.1 + 1 × 37.1 + 2 × 33.6 = 323.2 J/K, (mole × J/mole K = J/K). The total exhaust gas heat capacity from one mole propane combustion is (5×79/21)×29.1 + 3×37.1 + 4×33.6 = 793.1 J/K. The combustion enthalpies for Eqs. 7 and 8 are 890.8 and 2,219 kJ/mole, respectively [8]. If only the exhaust gas is heated and the changes of the heat capacities with temperature are omitted, the maximum exhaust gas temperature increase per combusting mole of fuel is 890.8×1000/323.2 = 2756 and 2219×1000/793.1 = 2798 K/mole for methane and propane, respectively. This indicates, thermodynamically, the substitution of methane with propane will not noticeably affect the unit combustion heat. It should be mentioned that if burned with pure oxygen, propane will produce a higher molar combustion heat because its exhaust gas is reduced by 5 × 79/21 = 18.8 moles of nitrogen. For methane, the total number of moles of exhaust gas will be reduced by only 2 × 79/21 = 7.5 moles. On the other hand, for the saturated straight-chain hydrocarbons as the number of carbon increases, its stability increases. That is, kinetically its ignition (combustion) becomes more difficult. Especially in the situation where the thermodynamic force is weak, such as insufficiency of reactant (oxygen), the kinetic effect becomes dominant. That is, some of propane molecules cannot be combusted fast enough in the combustion region near the surface of the ceramic tile of the burner. Most of these unburned hydrocarbons were transported with the emission gases from the burner top to the chimney and eventually completely consumed there. This has been observed in the study, and it is believed that the unburned propane led to the decreased radiant efficiency.

Effect of Hydrogen Addition on Radiant Efficiency

Hydrogen is mostly found in synthetic natural gases, where it can be 5%. Natural gas contains very little hydrogen. Adding hydrogen in the fuel was mainly for the purpose of simulating an operating condition which is close to lightback. Typical results from this experiment are shown in **Figure 13**, which illustrates that the hydrogen addition to the methane-air combustion increased the radiant efficiency. When reacted with oxygen in the air, hydrogen will have water as the final product:

$$\mathbf{H_2 + \tfrac{1}{2}\, O_2 = H_2O} \qquad \mathbf{(9)}$$

The combustion enthalpy for Eq. 9 is 241.8 kJ/mole [12]. Burning one mole of hydrogen in air, the maximum temperature increase is 241.8×1,000/(0.5 × 79/21 × 29.1 + 1 × 33.6) = 2,737 K/mole hydrogen. This is quite close to that from the combustion of methane. Therefore, the radiant efficiency should be similar to that of methane. However, probably like the propane combustion, the kinetic factor plays a critical role again. Hydrogen molecules have lower ignition activation energy than methane. They can be more quickly ignited and more thoroughly combusted in the combustion region near the surface of the burner, which leads to the higher radiant efficiency.

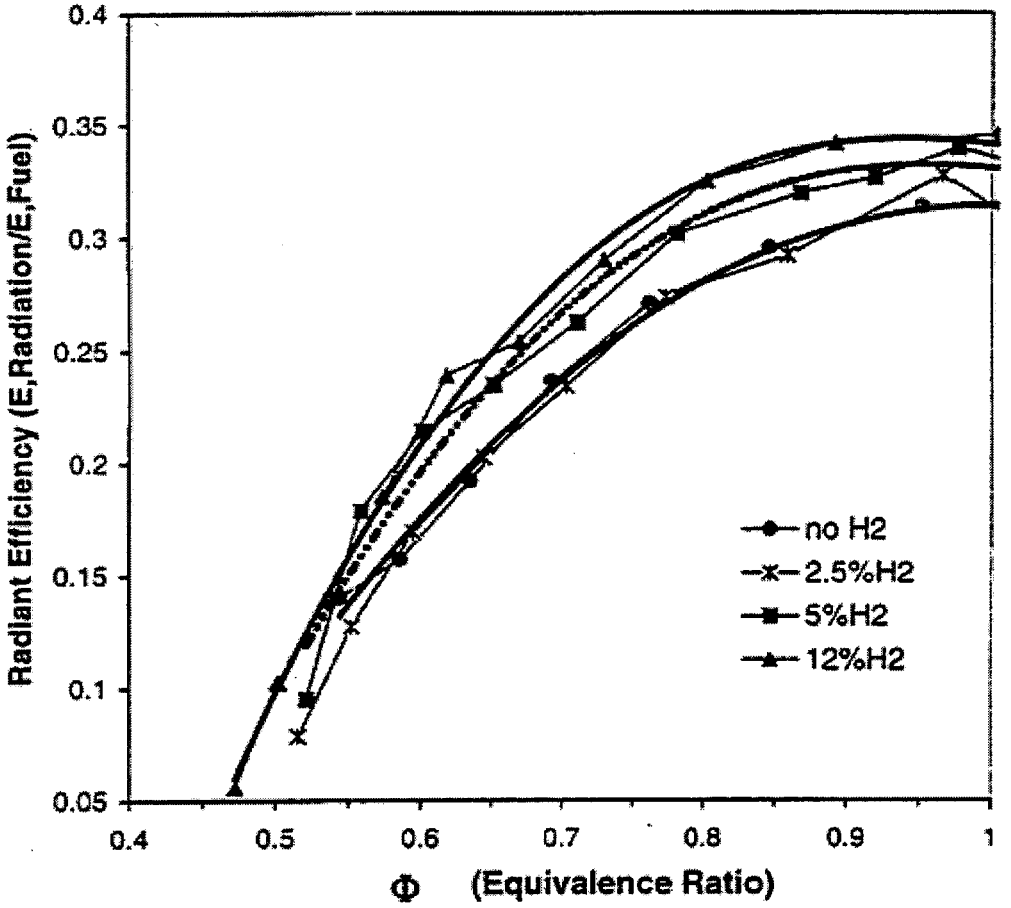

Figure 13. Effects of the H_2 Addition on the Radiant Efficiency

Emission Measurement

Radiant burners are known to have low pollutant emissions, especially NO_x emissions. This is mainly because the high radiant emission from the burner surface results in relatively low flame temperatures. As a consequence, it has been postulated that such burners produce NO_x mainly by the prompt-NO mechanism [13]. In the radiant combustor studied, the gas/air mixture is passed through a ceramic tile containing regularly spaced small holes. Combustion takes place in "valleys" between the ports, which enable the flame to spread over the whole tile surface area. The ceramic tile is then heated to incandescence. Usually in the radiant mode, the surface temperature is in the 1,100°C level. The changes of the gas compositions have significant impact on the emissions produced by the radiant combustor. Compared with radiant energy output, the compositions of the combustion exhaust gases were more sensitive to the changes of the combustion conditions.

Generally, the radiant burners operate at very high combustion efficiency. The CO_2 concentration in the exhaust gas can be used as an indicator of the combustion efficiency. Typical results of CO concentration in the exhaust flow are shown in **Figure 14** for the fuel-lean combustion region. It is seen that as the equivalence ratios Φ increased from 0.5 to 1, the concentrations of the CO_2 in the exhaust increased from 7.5% to more than 10%. At $\Phi = \sim 1$, where the stoichiometric fuel-air ratio for combustion was reached, the concentration of CO_2 arrived at its maximum, 10.7%. Theoretically, when a mole of CH_4 is completely combusted in air it will consume 2 moles of oxygen and produce one mole of CO_2 and 2 moles of water plus $2 \times 79/21$ moles of nitrogen. If the produced water vapor is not condensed, at the stoichiometric fuel-air ratio the CO_2 concentration in the combustion exhaust should be $1/(1+2+2\times79/21) = 9.5\%$. On the other hand, if the water vapor is completely condensed, the CO_2 concentration should be $1/(1+2\times 79/21) = 11.7\%$. It is believed that some of the water vapor was partially condensed in the sampling system which resulted in the maximum of 10.7% of the CO_2 concentration at the stoichiometric combustion.

In the fuel-lean combustion region, where the air was in excess, the concentration of O_2 was shown to proportionally decrease as the equivalence ratio increased until to about $\Phi = 1$, where the O_2 concentration reached its lowest point, ~ 0.2% (see **Figure 15**). After that, as the equivalence ratio further increased, the O_2 concentration did not effectively change but kept at about 0.2%.

In the case of the oxygen deficiency as in the fuel-rich combustion region, the CO concentration becomes significant. According to following equilibrium between CO_2 and CO,

$$\mathbf{CO_2 = CO + \tfrac{1}{2} O_2} \qquad \mathbf{(10)}$$

the concentration of CO is heavily dependent on the O_2 concentration. Since the equilibrium constant is very small, $K = 8.2\times10^{-46}$ at 298 K and 1.7×10^{-8} at 1200 K, respectively, the CO concentration will be very small if enough oxygen existed in the exhaust. The experimental results in **Figure 15** indicate that in the fuel-lean combustion region, because of the excess air, the CO concentration was kept in the a range from 240 to 320 ppm as Φ was increased from 0.75 to 1. As soon as the combustion was moved into the fuel-rich region, the CO concentration immediately jumped to 4,300 ppm at $\Phi = 1.02$. Since the instrumental measurement limitation for CO is 5,000 ppm, the higher CO concentration could not be determined.

Similar to the concentration of CO, the unburned hydrocarbon (UHC) is also an function of the O_2 concentration. As mentioned previously, the hydrocarbons that were not burned near the surface of the burner would be consumed further downstream along the exhaust passage of the burner. As a result, the measured unburned UHC concentration near the exit of the burner was quite close to equilibrium state. In the fuel-lean combustion region, the concentrations of the total unburned hydrocarbons were increased slowly from 100 to 300 ppm as Φ increased from 0.6 to 1, as shown in **Figure 16**.

NO_x is mainly the mixture of NO and NO_2, and they are formed in flame by different pathways, including the thermal mechanism, the prompt-NO route, and the nitrous oxide route [15][16][17]. Without getting involved into the detailed discussions about different chemical reaction mechanisms and elementary chemical reactions, the global reaction between the nitrogen and oxygen in the air can be simplified and described by following reactions [9]:

reaction between the nitrogen and oxygen in the air can be simplified and described by following reactions [9]:

$$N_2 + O_2 = 2\,NO \qquad (11)$$

$$NO + \tfrac{1}{2}\,O_2 = NO_2 \qquad (12)$$

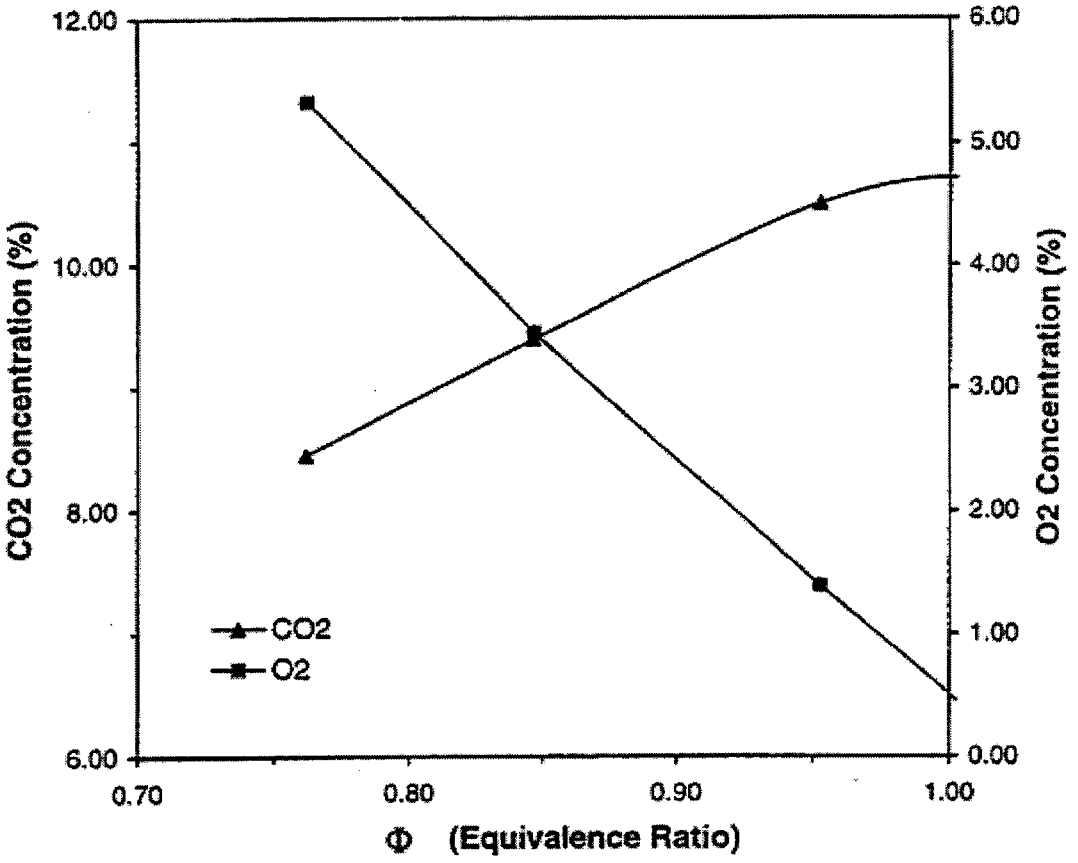

Figure 14. **CO_2 and O_2 Concentrations in the Combustion Emission Gas for the Different Equivalence Ratio (methane + air)**

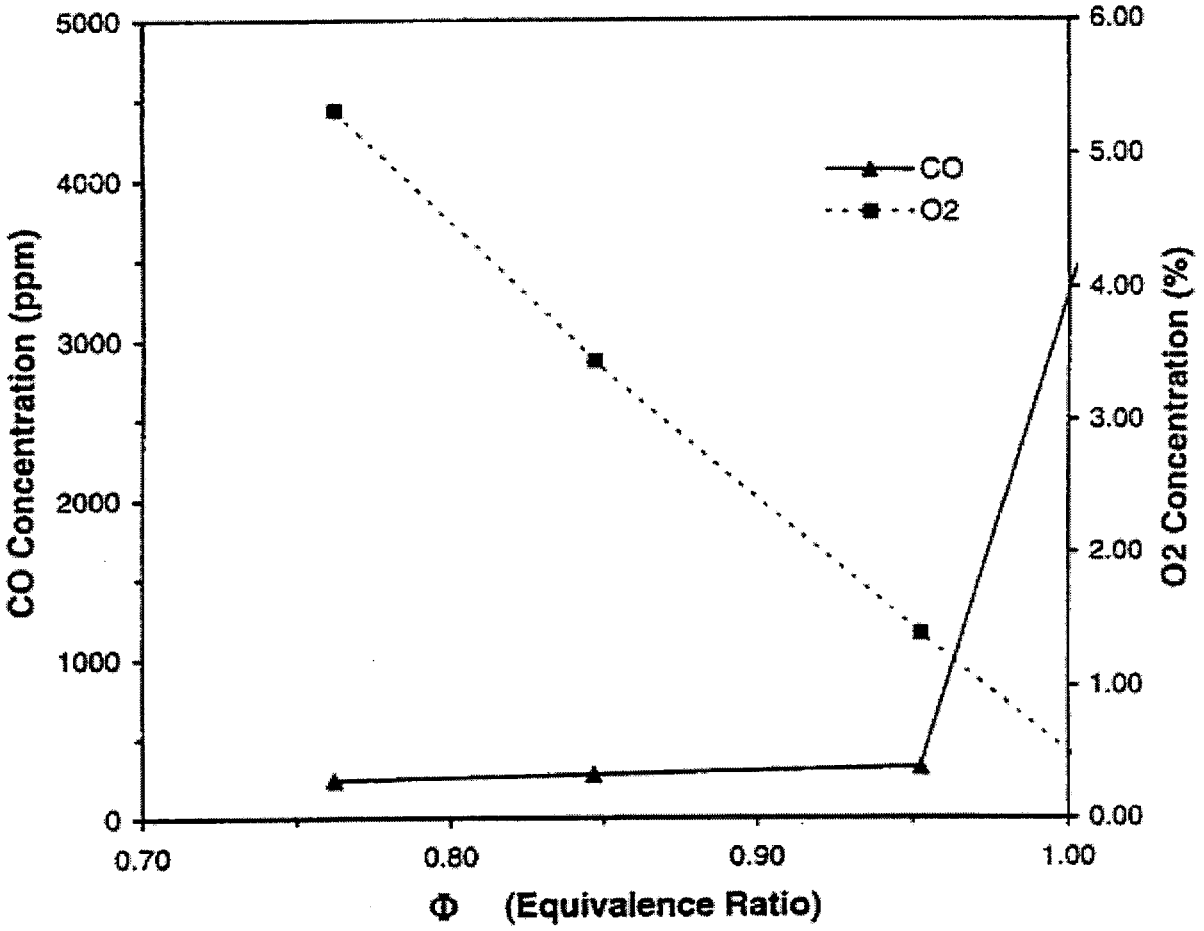

Figure 15. **CO and O_2 Concentrations in the Combustion Emission Gas for the Different Equivalence Ratio (methane + air)**

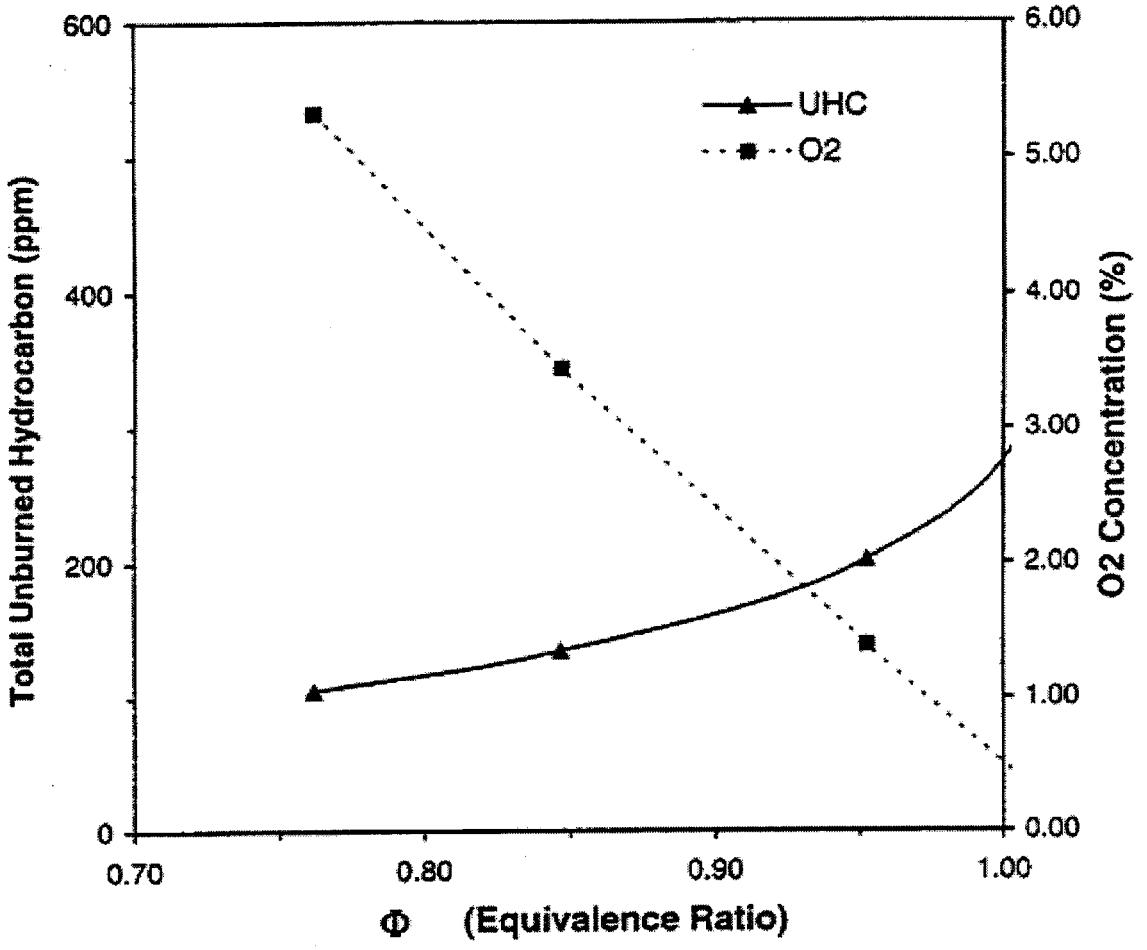

Figure 16. **Total Unburned Hydrocarbon (UHC) and O_2 Concentrations in the Combustion Emission Gas for the Different Equivalence Ratio (methane + air)**

Because Eqs. 11 and 12 are reversible reactions, NO_x concentration should be the function of oxygen concentration. However, **Figure 17** shows that, similar to CO_2, the NO_x concentration was heavily dependent on the equivalence ratio and had a maximum value at close to $\Phi = \sim 1$, ~7.5 ppm, except for that the NO_x curve reached its maximum value earlier than CO_2 did. There have been experimental and analytical results which indicated that unless there is a very large [O] atom overshoot for a considerable distance from the burner tile there is little thermal NO produced, and most of the NO is formed in the flame by the prompt-NO mechanism [18]. However, in most natural gas combustion cases, the formation rate of NO_x was found to be mainly controlled by the kinetic factors [13]. The concentrations of NO_x in the exhaust gases are mainly the function of combustion temperature as thermal NO_x mechanism is dominant. In the region of $\Phi = \sim 1$, the burner reached its highest temperature, and as the Φ went away from stoichiometric ratio to either side, the burner's temperature proportionally went down. It should be pointed out that the radiant burner did produce NO_x at a much lower level compared with other premixed combustors under similar equivalence ratio. It is believed that the intense radiation from the burner tile effectively reduced the flame zone temperature significantly, which in turn dramatically reduced the production of the thermal NO_x. In addition, because of its relatively uniform temperature distribution, the IR burner did not have spot areas that are at high temperatures. This exemplifies one of the advantages of IR radiant burners.

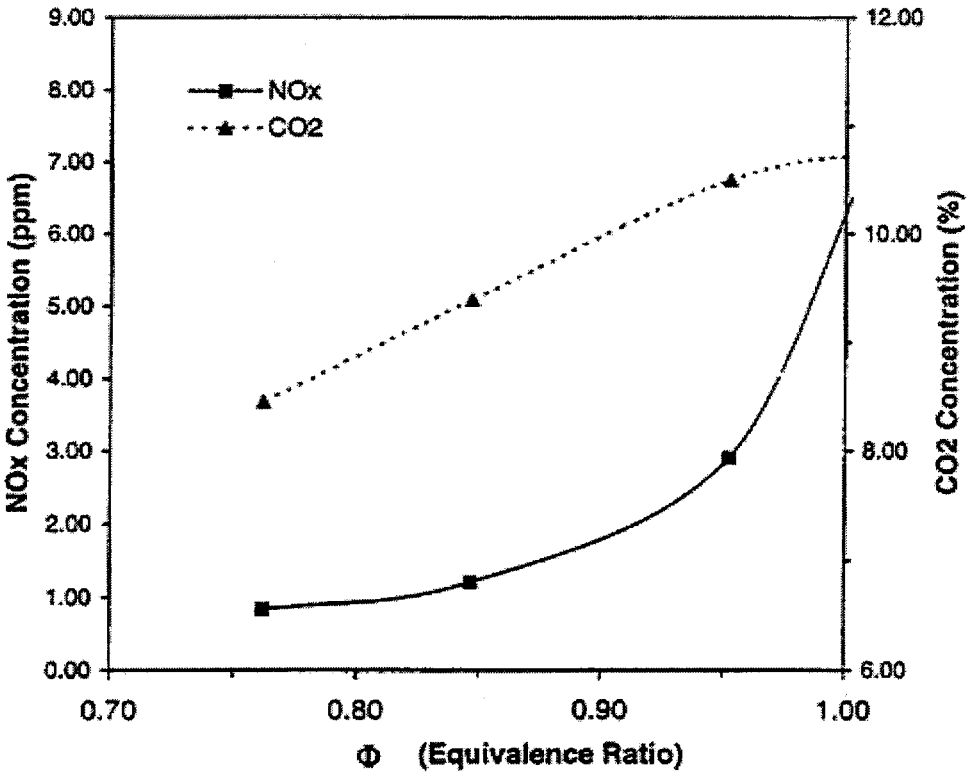

Figure 17. **NO_x and CO_2 Concentrations in the Combustion Emission Gas for the Different Equivalence Ratio (methane + air)**

In the following, the effects of fuel composition change upon the burner's emission performance are briefly summarized.

Effect of Nitrogen Addition on Emission

Typical emission measurement results obtained when nitrogen was added in the fuel is shown in **Figure 18.** It indicates that as the addition of nitrogen increased, the CO_2 concentration was decreased slightly but the maximum CO_2 concentration remained at close to stoichiometric equivalence ratio. This is because nitrogen is a non-combustible gas. When it was added to the methane-air combustion gas, it only worked as a dilutent. As the dilution increased, the concentration of the CO_2 decreased. The CO_2 concentration decrease also caused the equilibrium of Eq. 10 moved to the left-hand side, that is, the decrease of the CO concentration. Therefore the CO concentration in the exhaust gas shifted in relation to the equivalence ratio, as shown in **Figure 19.** The nitrogen addition reduced the combustion temperature, which in turn decreased the reaction rate. As a result, more unburned hydrocarbons should exist. However, these unburned hydrocarbons were believed to be burned out along the way to the exhaust pipe of the deep fat fryer. The total unburned hydrocarbon measured in the exhaust flow, shown in **Figure 20,** did not show significant change. **Figure 21** indicates some decrease of the NO_x concentration after nitrogen addition, which was caused by the decrease of the combustion temperature. As shown in the figure, an addition of 7% N_2 in the fuel caused the maximum NO_x to be reduced from around 7 ppm to less than 5 ppm.

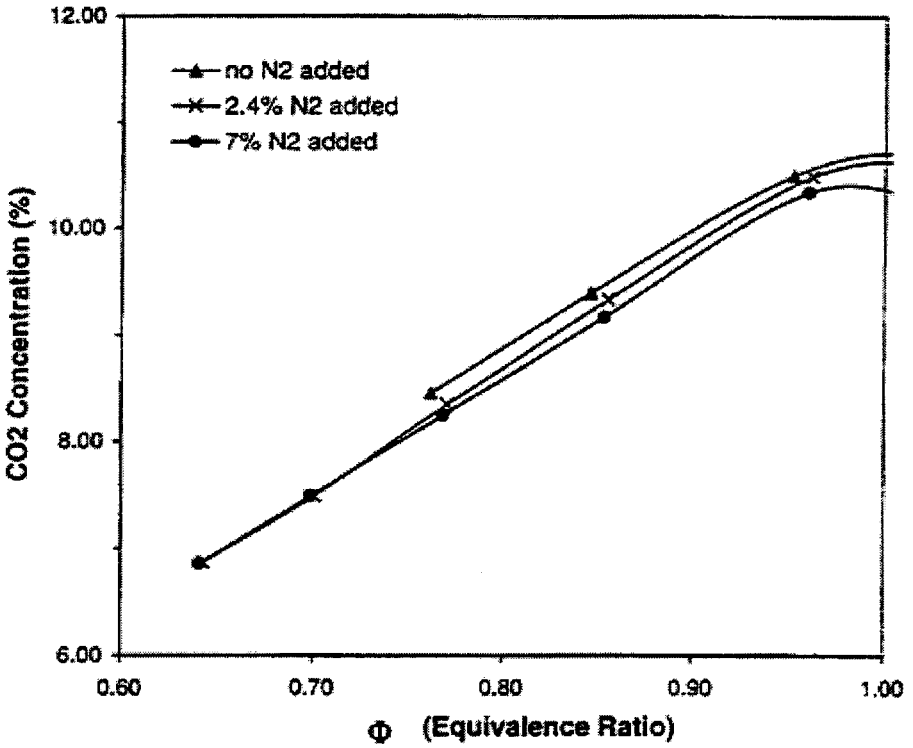

Figure 18. Effect of the N_2 Addition on the CO_2 Concentration in the Combustion Emission Gas

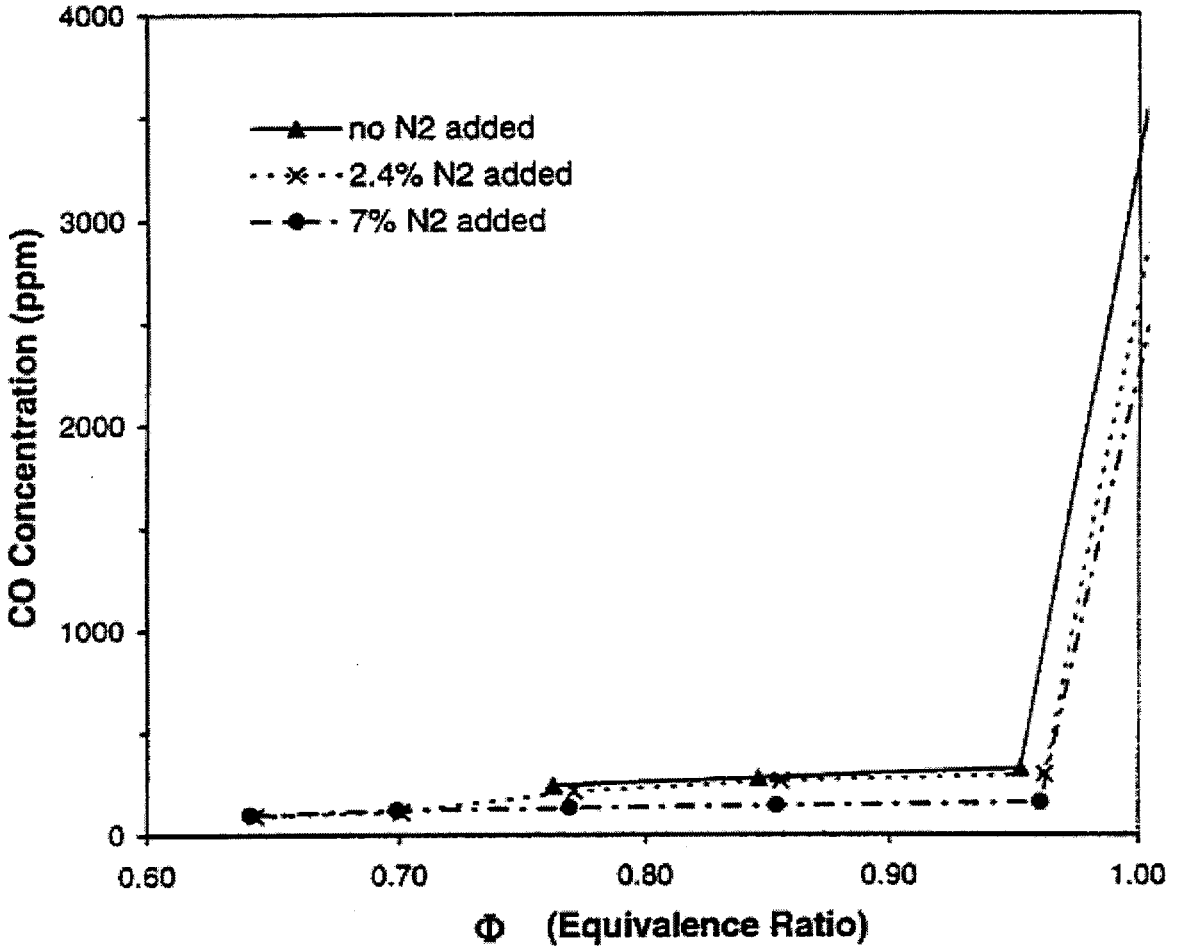

Figure 19. **Effect of the N_2 Addition on the CO Concentration in the Combustion Emission Gas**

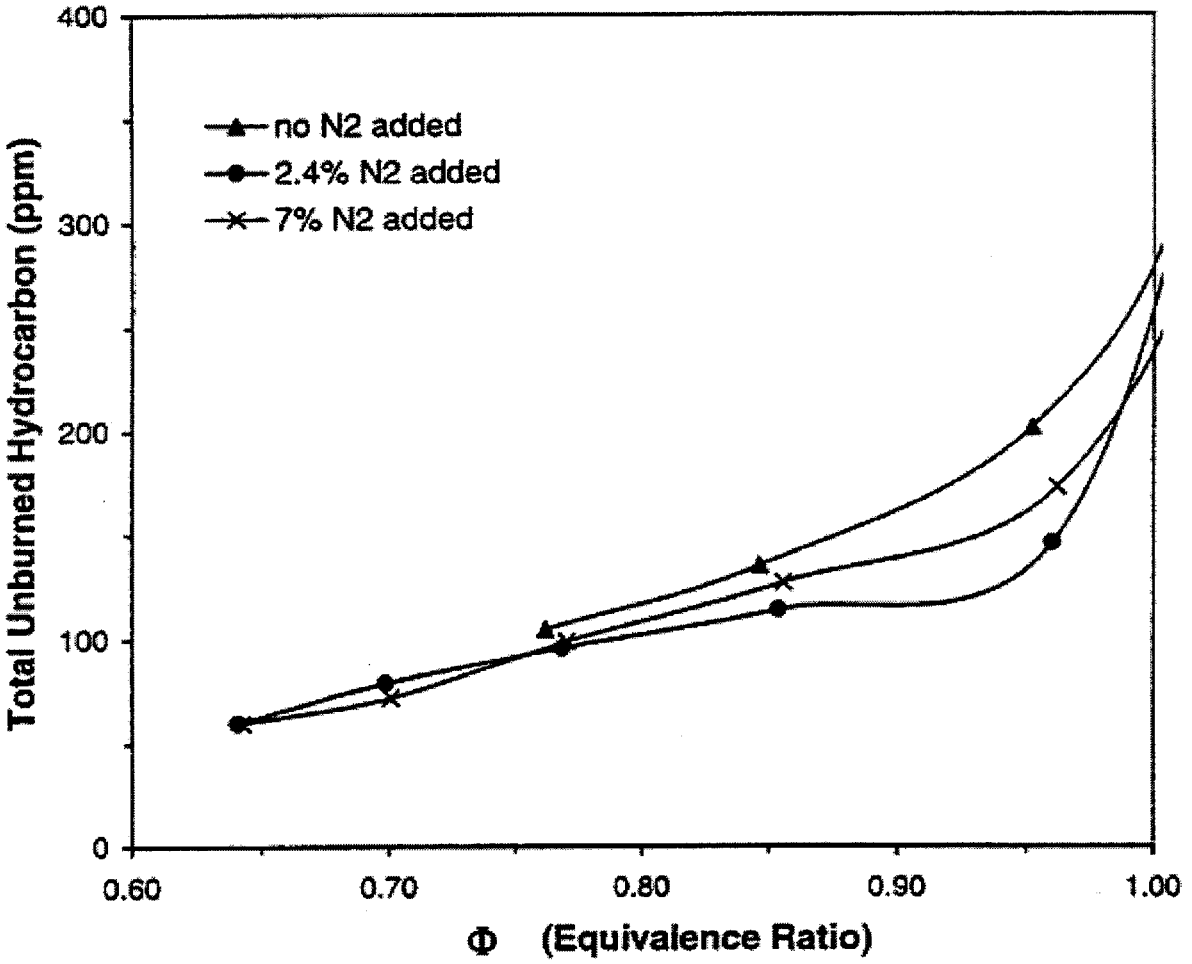

Figure 20. **Effect of the N_2 Addition on the Total Unburned Hydrocarbon Concentration in the Combustion Emission Gas**

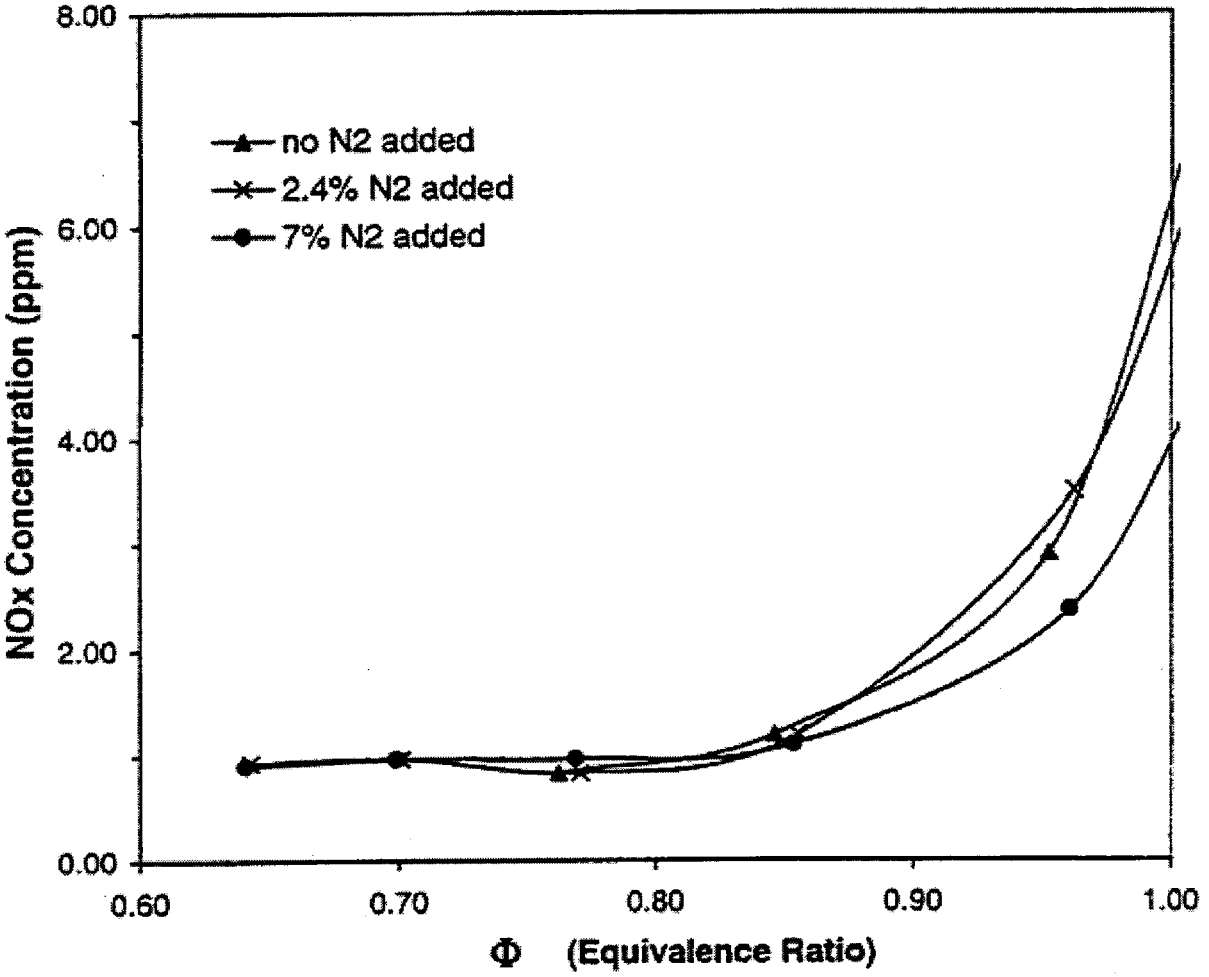

Figure 21. **Effect of the N_2 Addition on the NO_x Concentration in the Combustion Emission Gas**

Effect of Propane Addition on Emission

Addition of propane in the methane fuel significantly modified the emission characteristics of the combustor, especially the NO_x emissions. **Figure 22** shows that the CO_2 concentration curves shifted to the fuel-lean region as propane was added to the methane-air mixture. This confirmed the results and discussions from the radiation measurements. Because of propane's higher kinetic inertness, stronger thermodynamic condition, such as reactant oxygen, was needed for its reaction (combustion). **Figure 22** also indicates that the CO_2 maximum concentration for 18% propane addition was increased by about 0.2% compared to that of no propane addition. According to Eqs. 7 and 8, the CO_2 concentration produced for complete propane combustion is $3/(5\times79/21 + 3 + 4) = 11.6\%$ compared to 9.5% for the complete methane combustion. For the same kinetic reason, **Figure 23** illustrates that the CO curves also shifted to the fuel lean region. Similar to the nitrogen addition, most of the unburned hydrocarbons were burned on the way to the chimney. Therefore, the measurement results for total unburned hydrocarbon, shown in **Figure 24**, did not indicate significant change. Although, as discussed previously, propane did not increase the molar combustion heat; its addition did increase the total combustion heat. This resulted in the higher combustion temperature and significantly greater NO_x formation, as shown in **Figure 25**. As shown in the figure, when 18% propane was added to the methane, the maximum NO_x concentration in the exhaust flow was more than doubled, jumping from around 7 ppm to about 17 ppm. It can be concluded that when propane is used as peakshaving fuel, the NO_x emissions from natural gas applications will be increased significantly.

Effect of Hydrogen Addition on Emission

Hydrogen is widely considered "clean fuel" which generates much less pollutant emissions. The test results for the radiant burner confirmed this point of view. **Figure 26** shows that as hydrogen was added to the methane-air mixture, the CO_2 concentrations in the combustion emission gas went down. This is due to that there is no CO_2 formation from the H_2 combustion with oxygen in the air. The combustion products (H_2O and N_2) from the H_2 combustion worked in similar way as nitrogen. They only diluted the concentration of the CO_2 produced from methane/air combustion, which led to the decrease of CO_2 concentration in the exhaust. As the CO_2 concentration went down, the movement of the equilibrium of Eq. 10 resulted in the shift of the CO curve toward in the fuel-lean combustion, as shown in **Figure 27**. **Figure 28** illustrates that, similar as the situations of the propane and nitrogen addition, the hydrogen addition did not change the total unburned hydrocarbon concentrations significantly. Generally speaking, addition of hydrogen in the methane fuel will produce less NO_x in the exhaust gases, since hydrogen has a lower molar combustion. Typical results are shown in **Figure 29**, which indicates that the NO_x formation went down from around 7 ppm to 5.5 ppm due to reduced temperature when hydrogen was added.

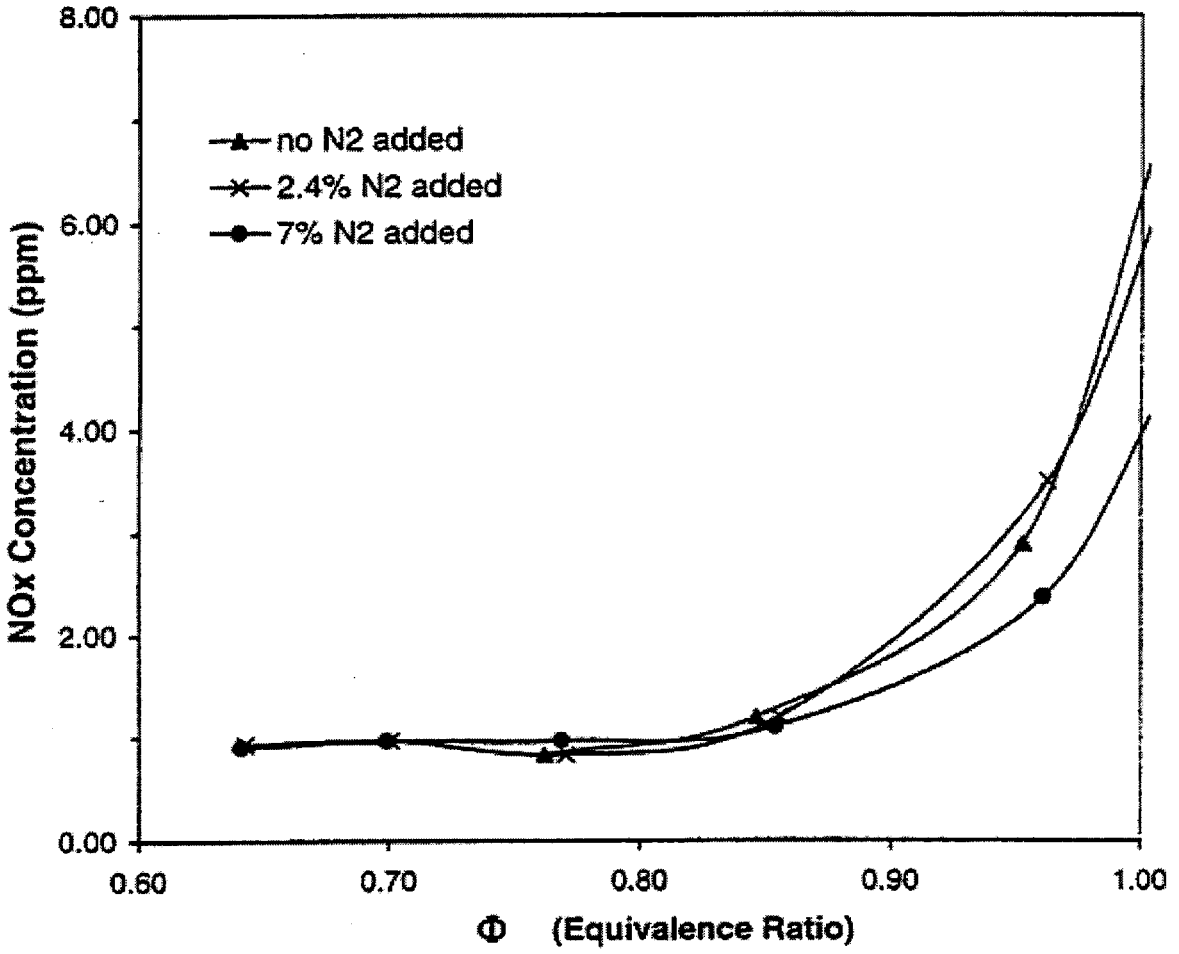

Figure 22. **Effect of the Propane Addition on the CO_2 Concentration in the Combustion Emission Gas**

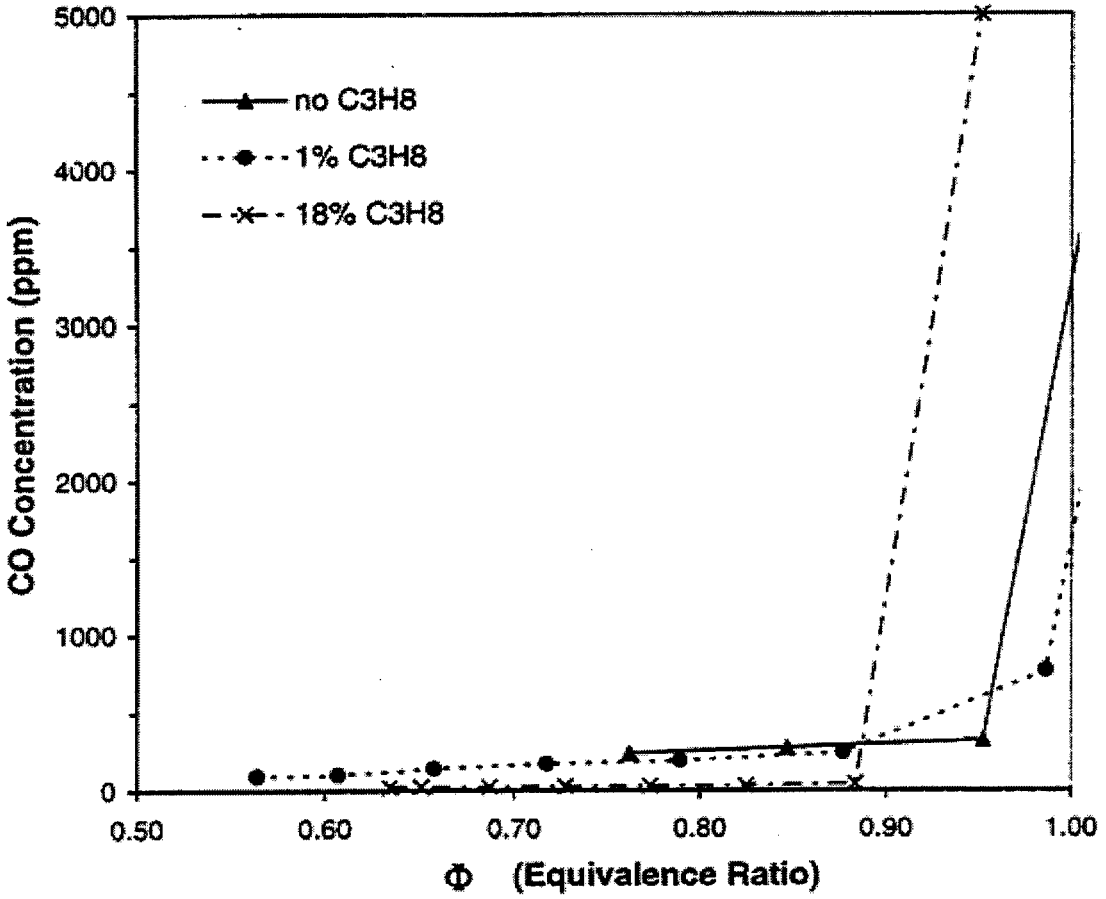

Figure 23. **Effect of the Propane Addition on the CO Concentration in the Combustion Emission Gas**

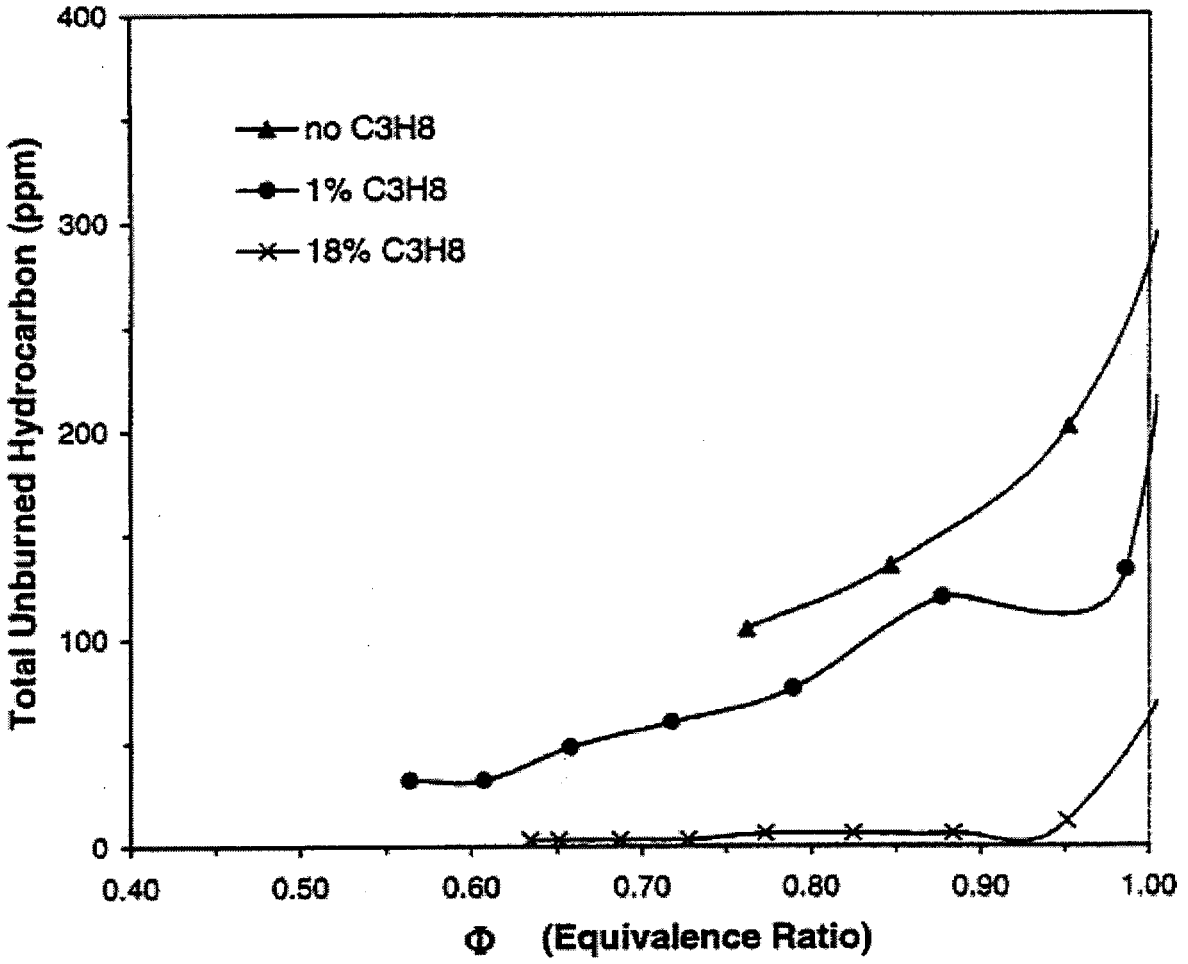

Figure 24. **Effect of the Propane Addition on the Total Unburned Hydrocarbon Concentration in the Combustion Emission Gas**

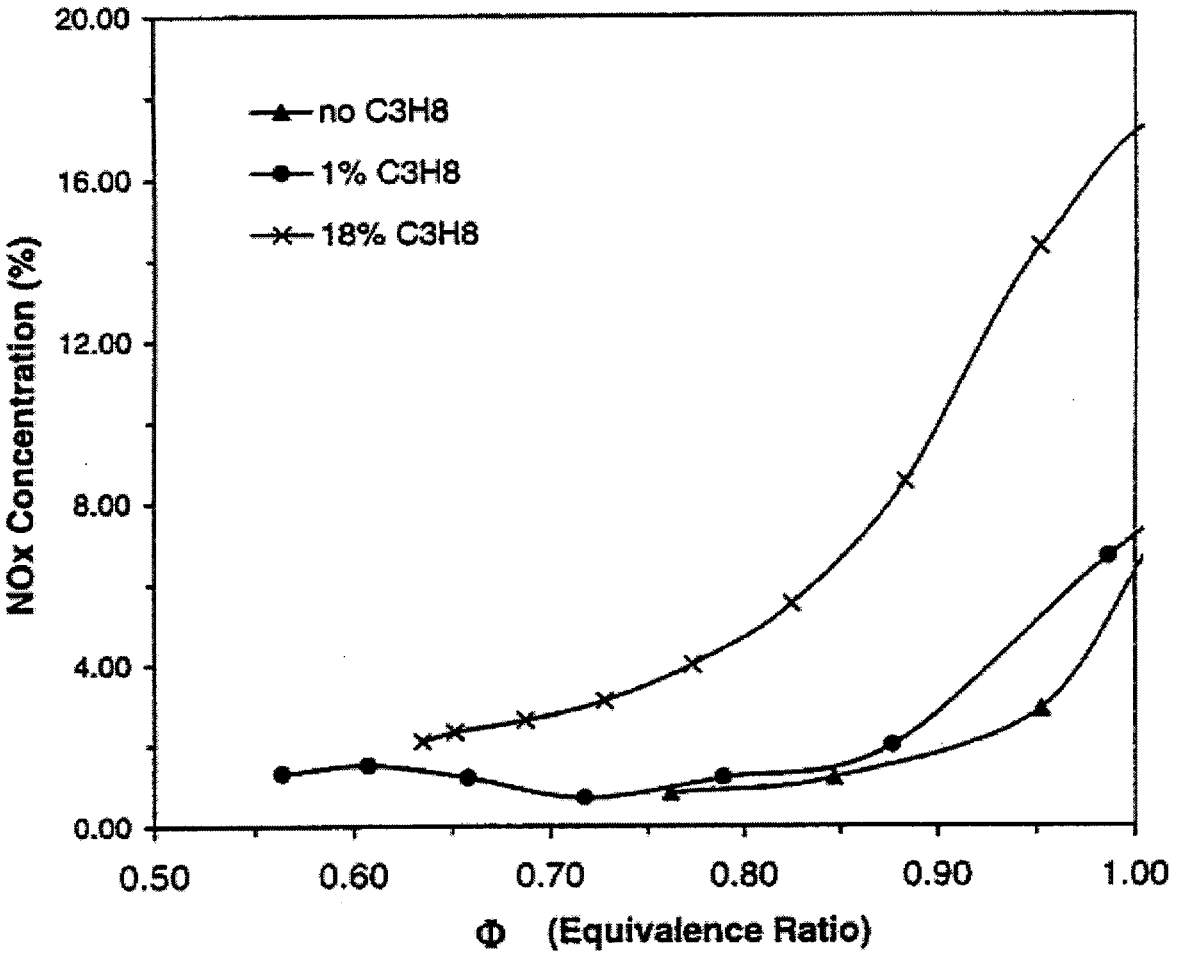

Figure 25. Effect of the Propane Addition on the NO_x Concentration in the Combustion Emission Gas

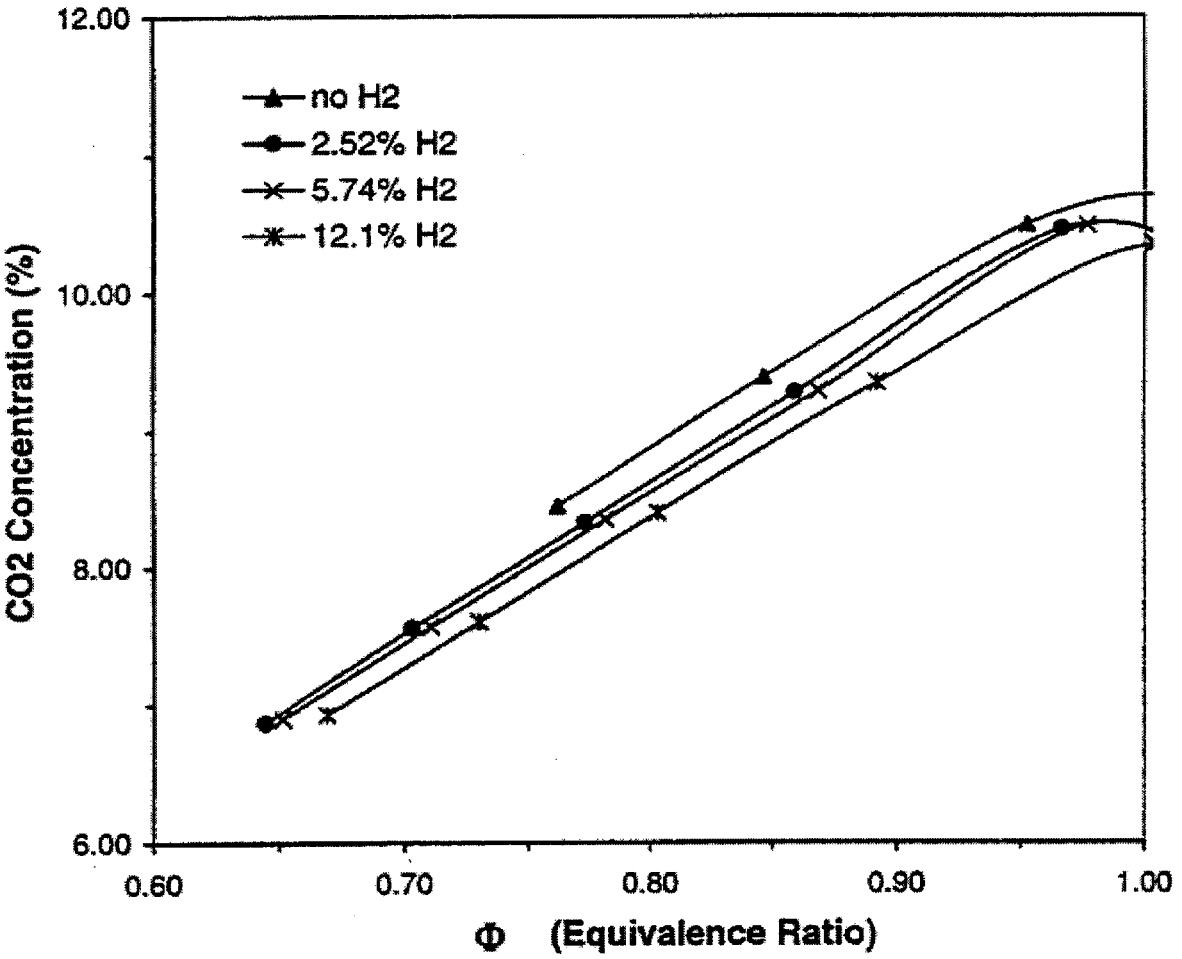

Figure 26. **Effect of the H_2 Addition on the CO_2 Concentration in the Combustion Emission Gas**

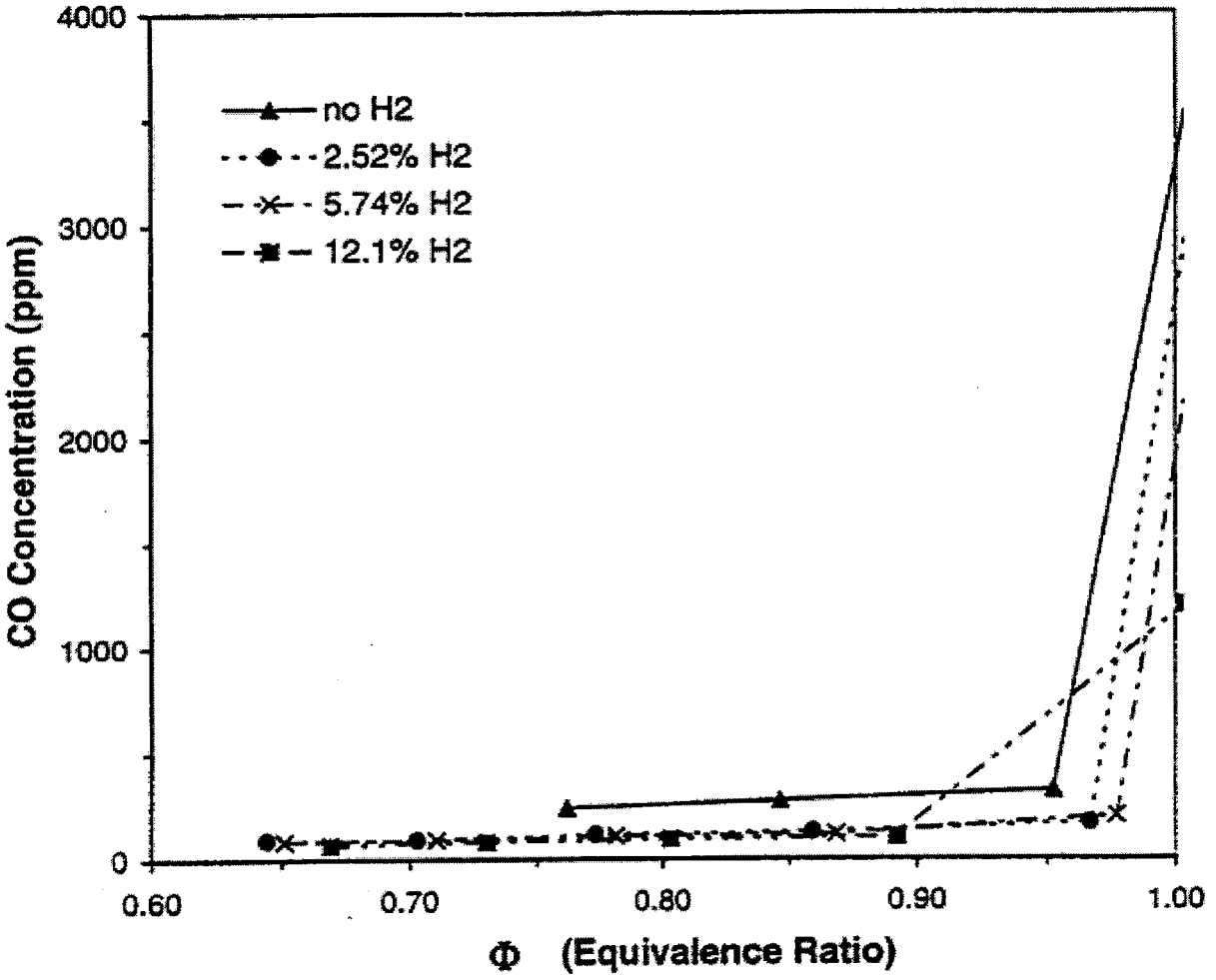

Figure 27. **Effect of the H_2 Addition on the CO Concentration in the Combustion Emission Gas**

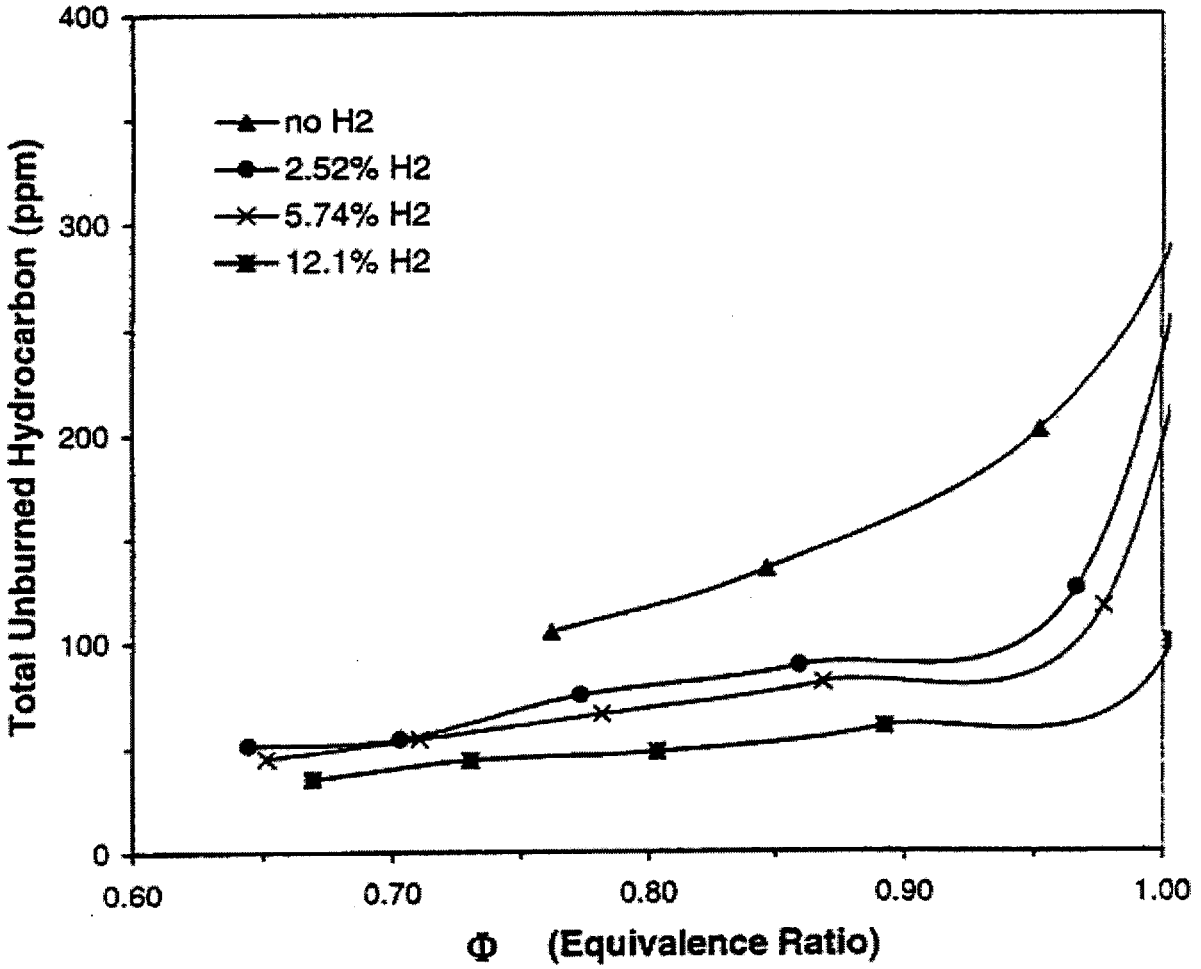

Figure 28. **Effect of the H_2 Addition on the Total Unburned Hydrocarbon in the Combustion Emission Gas**

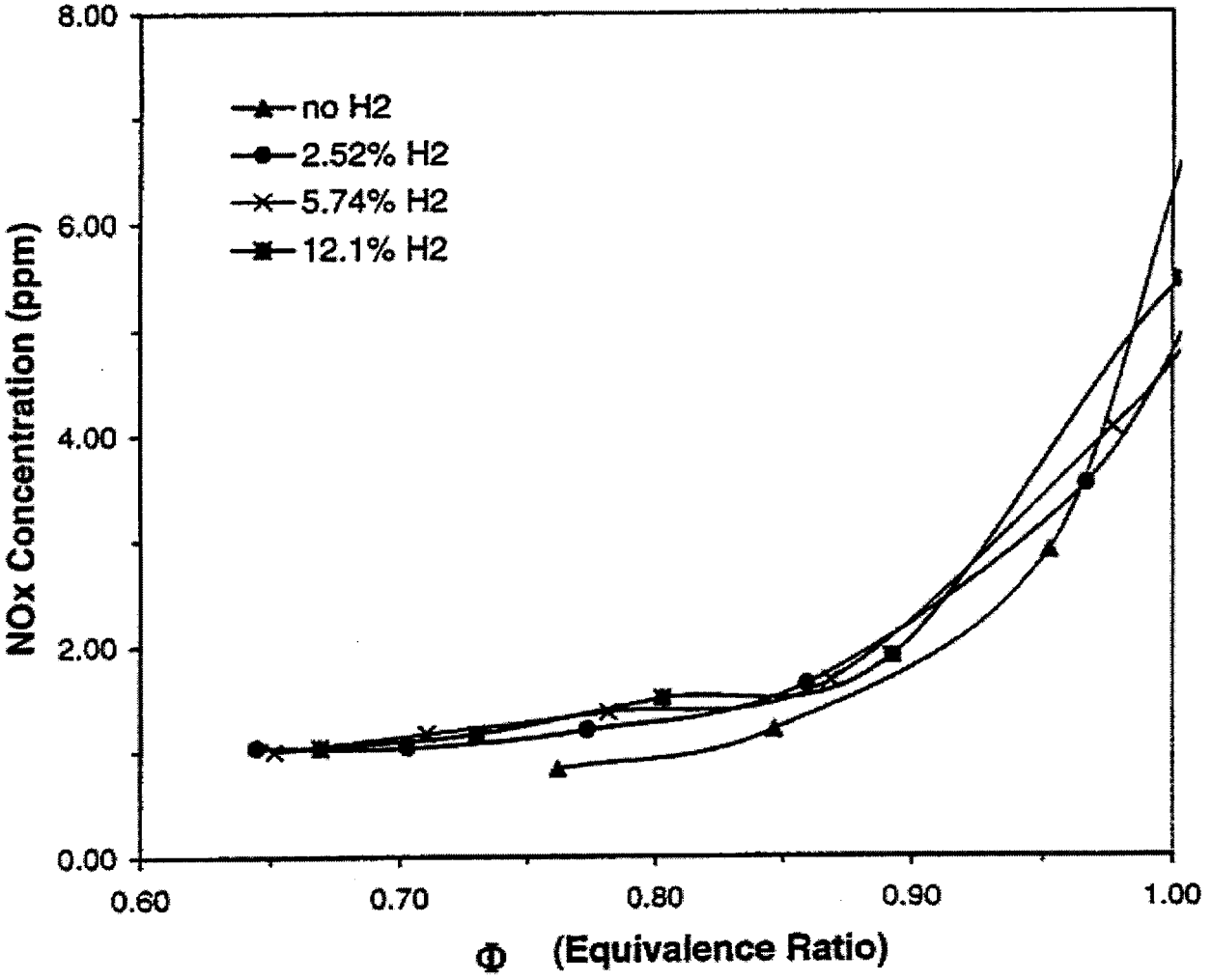

Figure 29. **Effect of the H_2 Addition on the NO_x Concentration in the Combustion Emission Gas**

Results From Altitude Tests

The modified deep fat fryer was operated on 100% methane at AGAR in Cleveland (about 600 ft) and altitude measurements were made at 4,350 ft above sea level. Data was also taken at a 6,800-ft elevation. Unfortunately the data taken was suspect due to rugged conditions of the laboratory and are not reported.

The CO_2, NO_x, CO, and flue gas temperature were measured using a Bacharach combustion analyzer. It was not possible to transport the FTIR used by CAU to the field sites, so an optical measurement of surface temperature with an Eppley optical pyrometer was used.

The results of the altitude test work are shown in **Figures 30** through **34**. The CO emission data shown in **Figure 30** is consistent with the data shown in **Figures 15, 19, 23,** and **27** with an asymptotic increase in CO as the equivalence ratio approaches 1. The normal operating range for this type of burner is in the equivalence ratio range of 0.6 to 0.8. The NO_x emissions data shown in **Figure 31** are consistent with the data shown in **Figures 17, 21, 25,** and **29**. The increasing NO_x emissions are largely a result of the higher tile temperature that are shown in **Figure 32**. In addition, the higher NO_x levels measured at the 600-ft. elevation seem to correlate with the higher tile temperatures shown in **Figure 32**. The elevated temperature increases the time/ temperature exposure of the products of combustion resulting in increased formation of NO_x. The decreasing flue gas temperature, shown in **Figure 33**, and the increasing thermal efficiency, shown in **Figure 34**, are consistent with the increasing radiant efficiency as shown in **Figure 10**.

The primary effect found of altitude was the decreased tile temperature which resulted in lower levels of NO_x emission. This is consistent with the analytical results as shown in **Figures 35** and **37**.

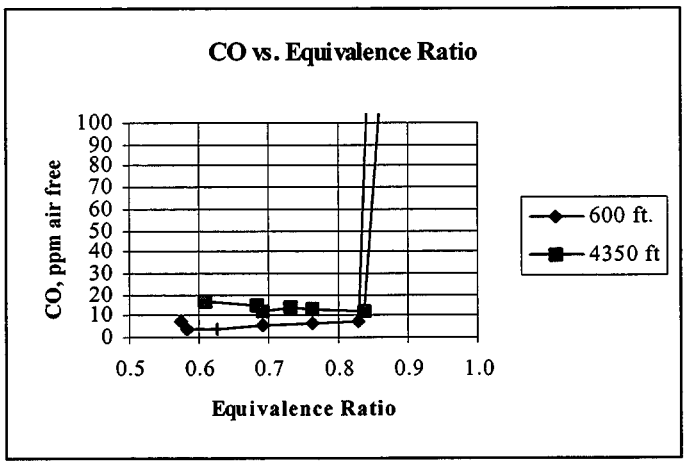

Figure 30. CO vs. Equivalence Ratio

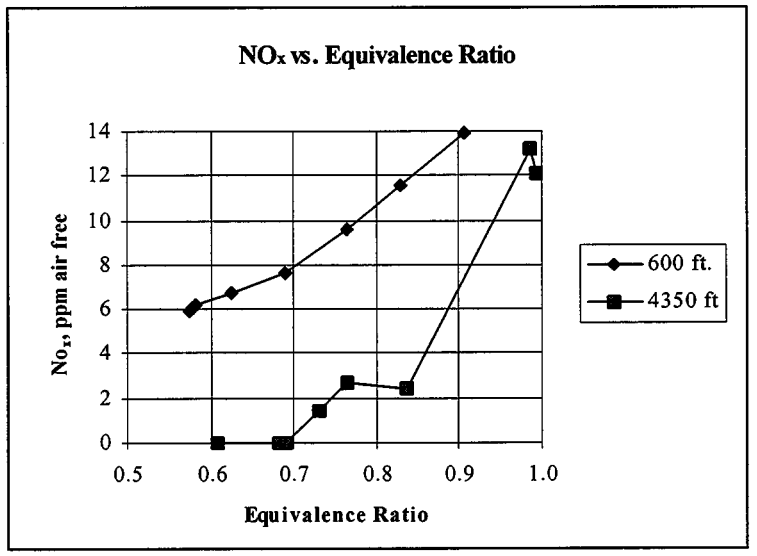

Figure 31. NO_x vs. Equivalence Ratio

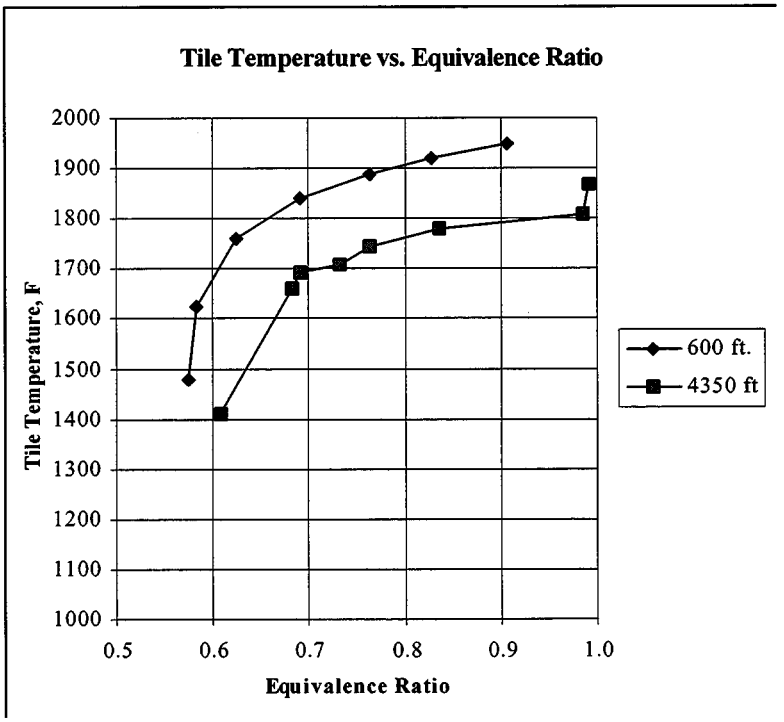

Figure 32. Tile Temperature vs. Equivalence Ratio

Error! Not a valid embedded object.

Figure 33. Flue Temperature vs. Equivalence Ratio

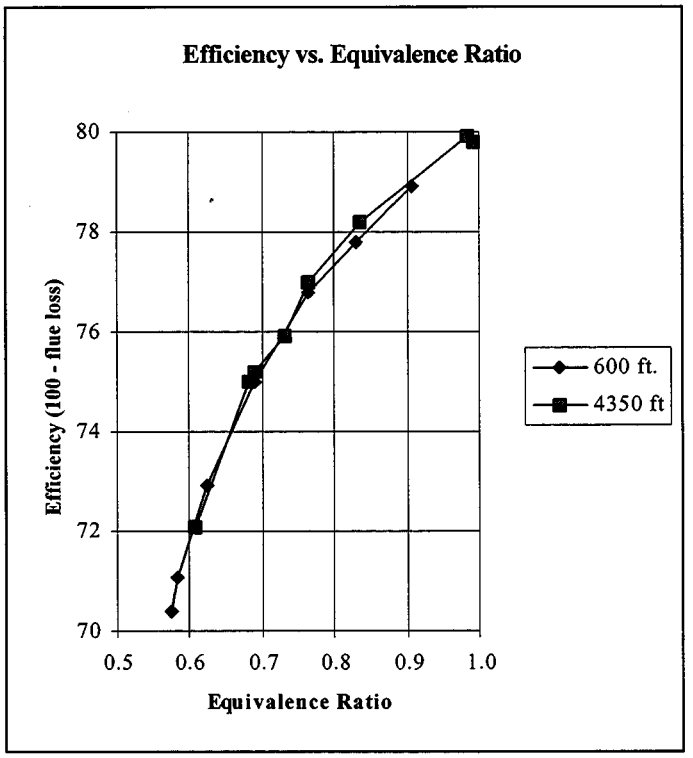

Figure 34. Efficiency vs. Equivalence Ratio

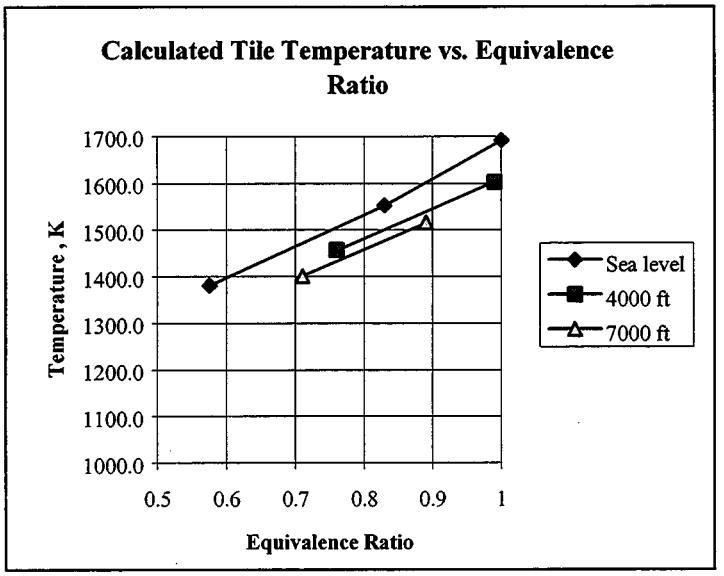

Figure 35. Calculated Tile Temperature vs. Equivalence Ratio

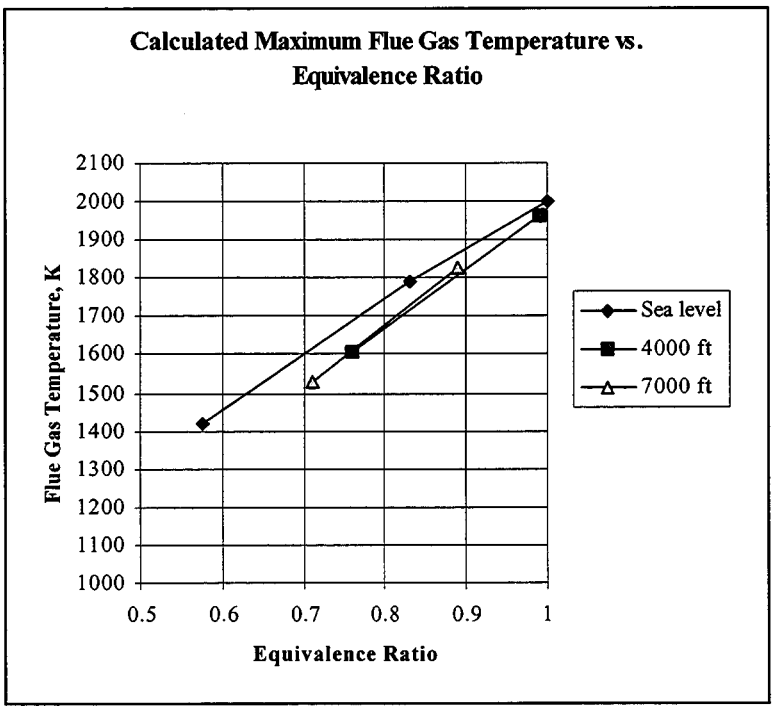

Figure 36. Calculated Maximum Flue Gas Temperature vs. Equivalence Ratio

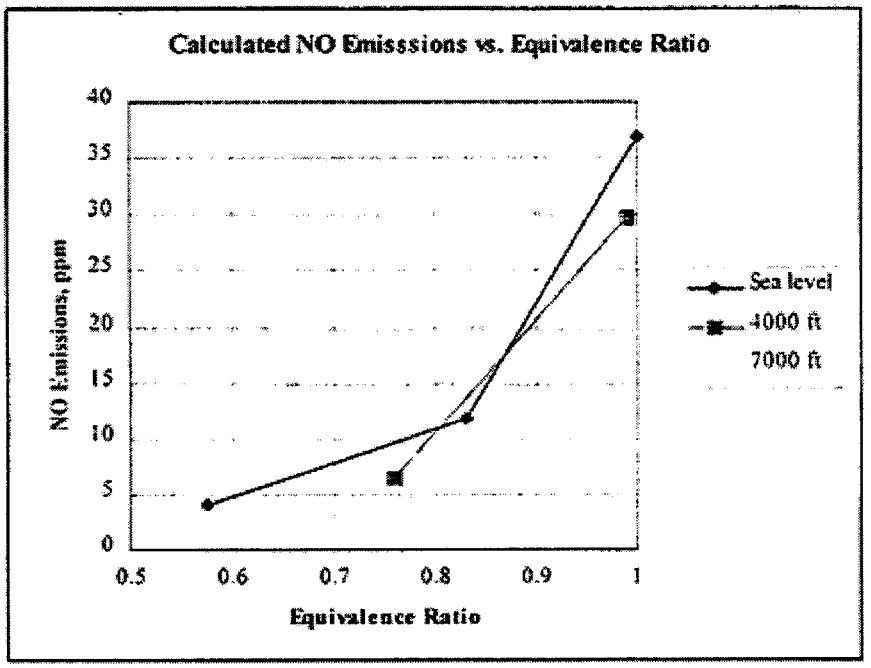

Figure 37. Calculated NO Emissions vs. Equivalence Ratio

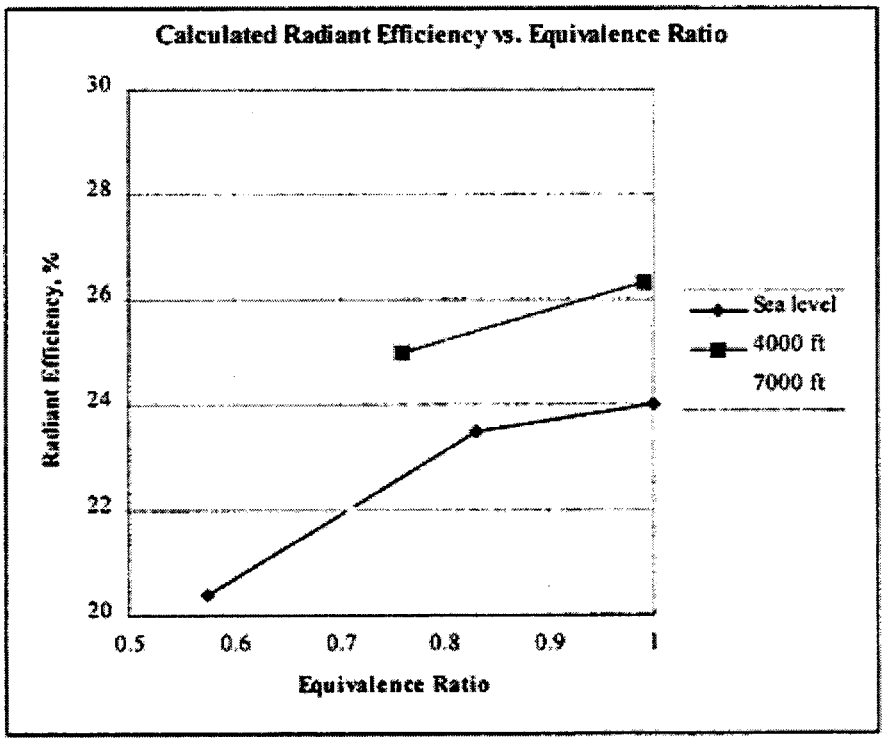

Figure 38. Calculated Radiant Efficiency vs. Equivalence Ratio

ANALYTICAL MODEL OVERVIEW

Over the years, there have been a variety of numerical models developed for predicting the performance of porous radiant burners (PRBs). The most sophisticated model reported in the literature was developed by Sathe et. al. (1990) at Arizona State University (ASU). The model developed at ASU couples the effects of convection, conduction, radiation, and combustion on the performance of PRBs. The flow is assumed to be one-dimensional, steady, laminar, and adiabatic. The solid matrix is assumed to be gray and to emit, absorb, and scatter radiant energy. Gaseous radiation is neglected compared to solid radiation. Non-local thermal equilibrium between the gas and the solid phase is accounted for by considering separate energy equations for the two phases.

The PRB model developed by Sathe et al. is based on a modified version of the PREMIX code developed at Sandia National Laboratory in the early 1980's. PREMIX is a subset of the CHEMKIN[1] solution routines and solves the governing equations for an adiabatic, one-dimensional, laminar premixed flame. Sathe et al. added the solid energy conservation equation and the radiative transfer equation to the PREMIX solution algorithm as well as modified the PREMIX gas phase energy equation to account for the thermal conduction heat transfer between the gas and solid burner. Sathe et al. accounted for the heat release and conversion of the methane into carbon dioxide and water using a simple single-step reaction mechanism. Details of the governing equations and solution algorithm can be found in the paper by Sathe et al.

In the current investigation, the model developed by Sathe et al. was acquired from ASU and modified extensively to account for detailed kinetics, pressure dependence, and improved binary diffusion model. The model was coupled with the most recent version of CHEMKIN which improved the capabilities of the model as well as the convergence stability. The GRImech 2.11 was used as the base chemical kinetic mechanism for all numerical simulations in this study. GRImech 2.11 contains the most up-to-date comprehensive methane oxidation and NO_x formation rate data available for the range of operating conditions investigated in this study. In order to model propane oxidation numerically, the three-step mechanism of Nguyen et al. (1989) was added to the GRImech 2.11 reactions.

Burner Geometry and Input Parameters

The PRB investigated in this study was a ported radiant used in a commercial deep fat fryer. This burner is different from the burners investigated by ASU which were typically high porosity fiber mat burners. The input parameters required by the model are shown in **Table 1**, along with the values used in the current investigation. The parameters for the PRB

[1] CHEMKIN is a software package whose purpose is to facilitate the formation, solution, and interpretation of problems involving elementary gas-phase chemical kinetics. The CHEMKIN library is a collection of about 100 highly modular FORTRAN subroutines that may be called to return information on equation of state, thermodynamic properties, and chemical production rates. The CHEMKIN package is also bundled with solution routines which solve the equations for perfectly stirred reactors (PSR), one dimensional laminar flames (PREMIX), or one-dimensional shocks (SHOCK).

were either taken from the manufacturer's literature, or estimated based on the physical parameters of the burner. The porosity and solid thermal conductivity were taken from the manufacturer's literature.

The convection heat transfer coefficient was calculated based on the physical parameters of the burner. The heat transfer surfaces of the ported PRB can be approximated as laminar flow through cylinders. The convection heat transfer coefficient, h, can be approximated as (Incropera and DeWitt, 1985):

$$h = \frac{48}{11}\frac{k}{D}$$

assuming constant heat flux. The diameter of the burner ports was measured to be 0.95 mm, and the manufacturer reported the thermal conductivity to be 0.329 W/m-K. The heat transfer coefficient based on these values is 1,511.2 W/m^{2}K. The actual value of the heat transfer coefficient used by the model is $h*a$, where a is the surface area per unit volume of the burner. a was estimated from the burner port diameter and the number of ports per unit surface area, and the thickness of the burner. The formula for calculating surface area per unit volume for cylinders through a solid is:

$$a = \frac{surfacearea}{volume} = \frac{2\pi rtn}{At}$$

where t is the burner thickness, A is the area of the burner tile, n is the number of ports in the burner tile, and r is the radius of the individual ports. This calculation accounts for the surface area provided by all the individual ports in the tile but neglects the top and bottom surfaces of the tile. The burner thickness was measured to be 1.5 cm, and the number of ports per square centimeter was measured to be approximately 35. Based on these numbers, the surface area per unit volume was estimated to be 10.4 cm^{-1}. This results in the ha value reported in **Table 1**.

The albedo and extinction efficiency were chosen for the solid material used in the burner and not the honeycomb structure. For the solid, the albedo was chosen to be very small, since the emissivity was approximated to be close to unity, and the extinction efficiency was chosen to be very large since the optical depth of the solid ceramic material is very large. The values chosen in **Table 1** were used for the simulations. Decreasing the extinction efficiency to a value of 2 and increasing the albedo to 0.5 affected the solution by less than 10%.

Table 1. Required Numerical Model Input Parameters

Input Parameter	Value
Solid Thermal Conductivity (W/mK)	0.329
Heat Transfer Coefficient, *ha* (W/m^3K)	$1.58x10^6$
Extinction Efficiency	40
Porosity	0.627
Albedo	0.01
Burner Thickness (cm)	1.5

MODEL RESULTS

Sixteen cases were selected to examine the effects of fuel composition, pressure, and fuel-air equivalence on pollutant (CO and NO) emissions from a porous radiant burner using the numerical model. The conditions which comprise each of the 16 test cases are shown in **Table 2**. The test cases may be grouped into four general categories: Cases 1 through 7 have a fuel composition of 100% methane and are used to determine the pressure and fuel-air equivalence ratio effects on emissions; Cases 8, 9, and 10 are used to assess the effects of hydrogen (H_2) addition; Cases 11 through 14 are used to assess the effects of nitrogen (N_2) addition; and Cases 15 and 16 are used to asses the effects of propane (C_3H_8) addition.

Tables 3 through **18** present the numerical modeling results for each of the 16 test cases. For each case, the predicted gas temperature, CO and NO emissions (expressed as ppmv on a wet, actual O_2 basis) are shown as a function of the distance above the burner surface. As the numerical model does not account for the addition (through mixing) of secondary (cooling) air downstream of the burner exit, presenting the results as a function of the distance above the burner surface allows for differentiating the amount of NO formed in the burner from that formed in the post-burner gases. Additionally for each test case, the predicted radiant efficiency of the burner is shown. It should be noted that due to the limited number of data points examined at a given fuel composition or fuel-air equivalence ratio, a tabular format was chosen for the results presentation rather than a graphical format which could give rise to misinterpretations through erroneous curve fitting.

A graphical presentation of the altitude results is shown in **Figures 35** to **38**.

From analysis of the numerical modeling results, the following general trends may be observed:

Effects of Fuel-Air Equivalence Ratio

The primary effect of decreasing the fuel-air equivalence ratio in lean combustion is to decrease the adiabatic flame temperature. As it has been well documented that NO formation under these conditions is exponentially dependent on temperature, it is not unexpected that the numerical modeling results of the PRB indicate the NO emissions are very sensitive to fuel-air equivalence ratio varying from 13.4 ppmv at the burner surface at

stoichiometric and atmospheric pressure to 3.9 ppmv at a fuel-air equivalence ratio of 0.575. Conversely, CO emissions are seen to decrease with decreasing fuel-air equivalence ratio. This too is as expected due to the fact that with leaner combustion more O_2 is available to oxidize CO to CO_2. Consistent with the experimental results, the numerical results also indicate that the radiant efficiency of the burner will fall off at the leanest equivalence ratios.

It should be noted that the model's lack of ability to account for the addition of cooling air downstream of the burner exit most significantly affects predicted NO emissions at the richest (near stoichiometric) conditions where the adiabatic flame temperature is the hottest, and significant amounts of NO form in the post-burner gases. At the leanest conditions examined, the gas temperature at the burner exit are cool enough not to permit additional NO formation in the post-burner region, and hence, the agreement with the experimental data is seen to be best at these leanest conditions.

Effects of Altitude

The numerical modeling results indicate that over the small pressure range examined (from 0.78, which is equivalent to 7,000 ft. altitude, to 1.0 atm) neither the NO nor the CO emissions exhibit a strong pressure dependence. At the conditions examined, neither the adiabatic flame temperature nor the predominant combustion free-radical concentrations (i.e., O-atom, H-atom, and OH-radical) should be strongly influenced by pressure, and hence, neither should the CO or NO formation chemistry. The radiant efficiency of the burner is seen to increase marginally with decreasing pressure, consistent with the experimental data taken at altitude. The temperature at the burner surface was seen to decrease marginally with decreasing pressure, which is also consistent with the experimental data taken at altitude

Effects of Hydrogen Addition

The primary effect of hydrogen addition to the methane fuel is on the adiabatic flame temperature. For example, the adiabatic flame temperature of a stoichiometric hydrogen-air flame at one atmosphere pressure is approximately 2,380 K; whereas, for a methane-air flame at the same conditions, the adiabatic flame temperature is only approximately 2,225 K. Comparing the results of Cases 8 (2.52% H_2) and 10 (12.13% H_2) (both at one atmosphere pressure and 0.9 fuel-air equivalence ratio), the predicted gas temperature at the burner surface is 1,593 and 1,615 K, respectively. This 23 K increase in temperature is reflected in the increased NO emission (10.3 ppmv (Case 10) versus 9.1 ppmv (Case 8)). The model results for predicted CO emission are not, however, as anticipated. For the conditions of Cases 8 and 10, the model predicts CO emissions of 19,891 and 20,442 ppmv, respectively. Case 10 with the increased level of hydrogen addition should be expected to yield a lower CO emission due to reduced level of carbon in the combined methane-hydrogen fuel. Likewise, the predicted model trend that the radiant efficiency decreases with increasing hydrogen addition is counter to that observed in the experimental results.

Effects of Nitrogen Addition

There is no significant amount of energy released during the oxidation of nitrogen. Thus, the effects of nitrogen addition are twofold: first acting as a dilutent, nitrogen directly reduces CO and NO emissions; and second, the addition of nitrogen causes a reduction in the adiabatic flame temperature. Comparing the results of Cases 11 (7.0% N_2) and 13 (2.37% N_2) (both at one atmosphere pressure and approximately 0.92 fuel-air equivalence ratio), the predicted gas temperature at the burner surface is 1,586 and 1,611 K, respectively. This 25 K decrease in temperature combined with the dilutent effect is reflected in the decreased NO emission (8.9 ppmv (Case 11) versus 10.6 ppmv (Case 13)). A decrease in the CO emission is also seen with increasing nitrogen addition (20,238 ppmv (Case 11) versus 22,413 ppmv (Case 13) at the burner surface). In addition to agreeing well with the general trends seen for CO and NO emission with N_2 addition, the numerical model also matches the experimental data with regard to the radiant efficiency. That is, the numerical model predicts that the radiant efficiency decreases with increasing nitrogen addition, and that amount of decrease in the radiant efficiency increases as the fuel-air equivalence ratio is decreased (24.5% versus 24.0% for Case 13 versus Case 11 at a fuel-air equivalence ratio of 0.92, but 21.2% versus 20.5% for Case 12 (7% N_2) versus Case 14 (2.37% N_2) at a fuel-air equivalence ratio of 0.5).

Effects of Propane Addition

Like the case of hydrogen addition, the primary effect of propane addition to the methane fuel is on the adiabatic flame temperature. For example, the adiabatic flame temperature of a stoichiometric propane-air flame at one atmosphere pressure is approximately 2,270 K; whereas, for a methane-air flame at the same conditions, the adiabatic flame temperature is only approximately 2,225 K. (As noted above, the adiabatic flame temperature for the hydrogen-air flame is 2,380 K, and hence, the effect of propane addition on flame temperature is expected to be less than that seen for the hydrogen addition cases.) Comparing the results of Cases 2 (0.0% C_3H_8) and 16 (18.18% C_3H_8) (both at one atmosphere pressure and 0.83 fuel-air equivalence ratio), the predicted gas temperature at the burner surface is 1,553 and 1,567 K, respectively. This 14 K increase in temperature produces only a marginally increased NO emission (7.5 ppmv (Case 16) versus 7.4 ppmv (Case 2)). This slight increase in NO is indeed found to be less than the increase associated with the hydrogen addition. The increased level of carbon in the combined methane-propane fuel is expected to result in a higher CO emission. This trend is seen in the numerical model results. At the burner surface, the CO emission with the Case 2 conditions (0.0% propane) is 14,451 ppmv, but 18,426 ppmv with the Case 16 (18.18% propane) conditions. The observed trend from the experimental results that propane addition does not greatly affect the radiant efficiency is also seen in the numerical results. The predicted radiant efficiency varies between 23.5% with no propane added to 24.0% with 18.18% propane added.

Table 2. Matrix of Operating Conditions Used With Numerical Model

Case Number	Fuel Composition (Molar Percent)	Pressure (atm)	Fuel-Air Equivalence Ratio
1	CH_4 (100%)	1.0	1.0
2	CH_4 (100%)	1.0	0.83
3	CH_4 (100%)	1.0	0.575
4	CH_4 (100%)	0.87	0.99
5	CH_4 (100%)	0.87	0.76
6	CH_4 (100%)	0.78	0.89
7	CH_4 (100%)	0.78	0.71
8	CH_4 (97.48%) H_2 (2.52%)	1.0	0.9
9	CH_4 (94.26%) H_2 (5.74%)	1.0	0.86
10	CH_4 (87.87%) H_2 (12.13%)	1.0	0.91
11	CH_4 (93%) N_2 (7%)	1.0	0.91
12	CH_4 (93%) N_2 (7%)	1.0	0.5
13	CH_4 (97.63%) N_2 (2.37%)	1.0	0.94
14	CH_4 (97.63%) N_2 (2.37%)	1.0	0.51
15	CH_4 (98.99%) C_3H_8 (1.01%)	1.0	0.51
16	CH_4 (81.82%) C_3H_8 (18.18%)	1.0	0.84

Table 3. Case 1 Numerical Modeling Results (fuel composition = 100% CH_4, pressure =1.0 atm, fuel-air equivalence ratio = 1.0)

Height above Burner Surface (cm)	CO (ppm)	NO (ppm)	Temperature (K)
0	26,978	13.4	1,642
1	8,661	29.1	1,969
2	6,886	33.6	1,990
3.5	5,886	36.9	2,003
Radiant Efficiency = 24.0%			

Table 4. **Case 2 Numerical Modeling Results (fuel composition = 100% CH4, pressure =1.0 atm, fuel-air equivalence ratio = 0.83)**

Height above Burner Surface (cm)	CO (ppm)	NO (ppm)	Temperature (K)
0	14,451	7.4	1,553
1	547	11.3	1,783
2	257	11.6	1,788
3.5	153	11.8	1,790
Radiant Efficiency = 23.5%			

Table 5. **Case 3 Numerical Modeling Results (fuel composition = 100% CH_4, pressure =1.0 atm, fuel-air equivalence ratio = 0.575)**

Height above Burner Surface (cm)	CO (ppm)	NO (ppm)	Temperature (K)
0	2,127	3.9	1,381
1	73	4.0	1,416
2	24	4.0	1,417
3.5	9.8	4.0	1,417
Radiant Efficiency = 20.4%			

Table 6. **Case 4 Numerical Modeling Results (fuel composition = 100% CH_4, pressure =0.87 atm, fuel-air equivalence ratio = 0.99)**

Height above Burner Surface (cm)	CO (ppm)	NO (ppm)	Temperature (K)
0	26,900	11.5	1,603
1	9,043	24.1	1,923
2	7,181	27.4	1,948
3.5	6,132	29.7	1,962
Radiant Efficiency = 26.3%			

Table 7. **Case 5 Numerical Modeling Results (fuel composition = 100% CH_4, pressure =0.87 atm, fuel-air equivalence ratio = 0.76)**

Height above Burner Surface (cm)	CO (ppm)	NO (ppm)	Temperature (K)
0	8,596	5.5	1,457
1	185	6.4	1,603
2	70	6.4	1,606
3.5	34	6.4	1,607
Radiant Efficiency = 25.0%			

Table 8. Case 6 Numerical Modeling Results (fuel composition = 100% CH_4, pressure =0.78 atm, fuel-air equivalence ratio = 0.89)

Height above Burner Surface (cm)	CO (ppm)	NO (ppm)	Temperature (K)
0	20,321	6.8	1,516
1	1,939	12.9	1,808
2	1,024	13.7	1,821
3.5	631	14.1	1,827
Radiant Efficiency = 28.3%			

Table 9. Case 7 Numerical Modeling Results (fuel composition = 100% CH_4, pressure =0.78 atm, fuel-air equivalence ratio = 0.71)

Height above Burner Surface (cm)	CO (ppm)	NO (ppm)	Temperature (K)
0	6631	4.5	1401
1	353	4.8	1526
2	135	4.9	1527
3.5	69	4.9	1528
Radiant Efficiency = 22.0%			

Table 10. Case 8 Numerical Modeling Results (fuel composition = 97.48% CH_4 and 2.52% H_2, pressure =1.0 atm, fuel-air equivalence ratio = 0.9)

Height above Burner Surface (cm)	CO (ppm)	NO (ppm)	Temperature (K)
0	19,891	9.1	1,593
1	1,796	18.1	1,886
2	1,004	19.6	1,897
3.5	663	20.6	1,902
Radiant Efficiency = 23.6%			

Table 11. Case 9 Numerical Modeling Results (fuel composition = 94.26% CH_4 and 5.74% H_2, pressure =1.0 atm, fuel-air equivalence ratio = 0.86)

Height above Burner Surface (cm)	CO (ppm)	NO (ppm)	Temperature (K)
0	17,580	7.3	1,566
1	876	13.3	1,833
2	443	14.0	1,840
3.5	277	14.3	1,843
Radiant Efficiency = 23.6%			

Table 12. **Case 10 Numerical Modeling Results (fuel composition = 87.87% CH_4 and 12.13% H_2, pressure =1.0 atm, fuel-air equivalence ratio = 0.91)**

Height above Burner Surface (cm)	CO (ppm)	NO (ppm)	Temperature (K)
0	20,442	10.3	1,615
1	2,467	21.8	1,923
2	1,461	24.2	1,937
3.5	1,002	25.9	1,943
Radiant Efficiency = 21.7%			

Table 13. **Case 11 Numerical Modeling Results (fuel composition = 93.0% CH_4 and 7.0% N_2, pressure =1.0 atm, fuel-air equivalence ratio = 0.91)**

Height above Burner Surface (cm)	CO (ppm)	NO (ppm)	Temperature (K)
0	20,238	8.9	1,586
1	1,893	17.6	1,879
2	1,065	19.1	1,889
3.5	703	20.0	1,895
Radiant Efficiency = 24.0%			

Table 14. **Case 12 Numerical Modeling Results: Fuel Composition = 93.0% CH_4 and 7.0% N_2, Pressure =1.0 atm, Fuel-Air Equivalence Ratio = 0.5**

Height above Burner Surface (cm)	CO (ppm)	NO (ppm)	Temperature (K)
0	1,067	1.8	1,242
1	123	1.8	1,253
2	47	1.8	1,254
3.5	23	1.8	1,254
Radiant Efficiency = 20.5%			

Table 15. **Case 13 Numerical Modeling Results (fuel composition = 97.63 % CH_4 and 2.37% N_2, pressure =1.0 atm, fuel-air equivalence ratio = 0.94)**

Height above Burner Surface (cm)	CO (ppm)	NO (ppm)	Temperature (K)
0	22,413	10.6	1,611
1	3426	22.7	1,924
2	2,160	25.5	1,940
3.5	1,541	27.5	1,948
Radiant Efficiency = 24.5%			

Table 16. **Case 14 Numerical Modeling Results (fuel composition = 97.63 % CH_4 and 2.37% N_2, pressure =1.0 atm, fuel-air equivalence ratio = 0.51)**

Height above Burner Surface (cm)	CO (ppm)	NO (ppm)	Temperature (K)
0	755	2.0	1,256
1	97	2.0	1,265
2	38	2.0	1,266
3.5	20	2.0	1,266
Radiant Efficiency = 21.2%			

Table 17. **Case 15 Numerical Modeling Results (fuel composition = 98.99% CH_4 and 1.01% C_3H_8, pressure =1.0 atm, fuel-air equivalence ratio = 0.51)**

Height above Burner Surface (cm)	CO (ppm)	NO (ppm)	Temperature (K)
0	989	1.7	1,235
1	129	1.7	1,246
2	53	1.7	1,247
3.5	31	1.7	1,247
Radiant Efficiency = 21.1%			

Table 18. **Case 16 Numerical Modeling Results (fuel composition = 81.82% CH_4 and 18.18% C_3H_8, pressure =1.0 atm, fuel-air equivalence ratio = 0.84)**

Height above Burner Surface (cm)	CO (ppm)	NO (ppm)	Temperature (K)
0	18,426	7.5	1,567
1	1,026	13.9	1,840
2	527	14.7	1,847
3.5	331	15.1	1,850
Radiant Efficiency = 24.0%			

DISCUSSION AND CONCLUSIONS

Following conclusions can be obtained from the experimental results:

- Fourier transform infrared spectroscopy (FTIR) is a simple, fast, reliable, and nondestructive analytical method for infrared burner radiation studies. By using the method developed at Clark Atlanta University, consistent and reliable infrared spectral results can be obtained. An accurate radiant energy can be calculated from these infrared spectra using a blackbody as the calibration standards.

the IR burner produced its maximum radiation efficiency, ~31.4%. At the same time, the concentration of CO_2 in the exhaust gas reached its maximum value, ~ 10.7%. In the fuel-lean region, the O_2 concentration in the emission gas decreased proportionally as Φ increased, but the concentrations of CO and UHC were kept in a couple of hundred ppm ranges. The NO_x formation was mainly dependent on the combustion temperature, and reached its maximum, ~8 ppm, at Φ = ~1. Because of the relatively low and uniform temperature distribution, the IR burner produced lower NO_x than traditional gas burners.

- Addition of nitrogen in the methane fuel produced lower radiant efficiency. Nitrogen is a non-combustible gas. It worked only as dilutent. This trend was observed both experimentally and analytically.

- Addition of propane in the methane fuel produced similar radiant efficiency with much higher NO_x emissions.

- Addition of hydrogen in the methane fuel produced similar radiant efficiency as the methane fuel without significant effect on the production of NO_x, CO_2, and CO.

- The primary effect found of altitude was the decreased tile temperature which resulted in lower levels of NO_x emission. This trend was observed both experimentally and analytically.

ACKNOWLEDGMENTS

This work was supported by the U.S. Department of Energy, through Contract No. DE-FG22-94MT94011, and a consortium of natural gas local distribution companies consisting of Atlanta Gas Light Company, Brooklyn Union Gas Company, Columbia Gas Distribution Company, and National Fuel Gas Distribution Corporation. The assistance of Mountain Fuel Supply Company in providing the experimental facility for the altitude work is also appreciated.

REFERENCES

1. "Basic Research on Radiant Burners," Final Report, February 1987 - February 1992, Gas Research Institute, 8600 West Bryn Mawr Avenue, Chicago, Illinois 60631.

2. Liss, W. H. Thrasher, and G.F. Steinmetz, "Variability of Natural Gas Composition in Select Major Metropolitan Areas of the United States," GRI-92/0123, March 1992.

3. "A Study of Infra-Red Energy Generated by Radiant Bas Burners," Research Bulletin 92, American Gas Association Laboratories, November 1962.

4. Taylor, J.H.; Benedict, W.S. and Strong, J.; *J Chem. Phys.*, 20, 1952, p. 1884.

5. Nakamoto, K.; *Infrared Spectra of Inorganic and Coordination Compounds*, 2ed ed., John Wiley & Sons Inc., New York, 1970, p. 17-18, 83.

6. *CRC Handbook of Basic Tables for Chemical Analysis*, p. 519.

7. Golombok, M., and Shirvill, L.C., "Radiation Characteristics of Surface Combustion Burners," Shell Research Ltd., Thornton Research Center, TCRP 3925, Eurotherm Conference, Cascais, Portugal, October 8-10, 1990.

8. Dird, R.B.; Stewart, W.E. and Lightfoot, E.N.; *Transport Phenomena*, John Wiley & Sons Inc., New York, 1960, p. 427-437.

9. Plank, M.; *Vorlesungen uber die Theorie der Warmestrahlung*, 5th ed., Barth Leipzig, 1923.

10. Dorf, R.C., ed.; *The Engineering Handbook*, CRC Press Inc., Boca Raton, 1996, p.518-520.

11. Lide, D.R., ed.; *CRC Handbook of Chemistry and Physics*, 73rd ed., CRC Press Inc., Boca Raton, 1992, p.10-300 - 10-301.

12. Nevers, N. de; *AIR POLLUTION CONTROL ENGINEERING*, McGraw-Hill Inc., New York, 1995, p.378-393, 416.

13. Bai "Study of The Effects of Ambient Conditions upon the Performance of Fan Powered, Infrared, Natural Gas Burners," Quarterly Technical Progress Reports, DOE Grant No. DE-FG22-94MT94011, 1994-1997.

14. Kee, R.J., Miller, J. A., Evans, G. H., and Dixon Lewis, G., Twenty-second Symposium (International) on Combustion, The Combustion Institute, Pittsburgh, 1988, p. 1479.

15. Bowman, C. T., Prog. Ener. Combust. Sci. 1:31, 1975.

16. De Soete, G.G., Fifteenth Symposium (International) on Combustion, the Combustion Institute, Pittsburgh, 1974. P. 1093.

17. Corr, R. A., Malte. P. C., and Mrinov, Poster Presentation P10, Twenty-third Symposium (International) on Combustion, the Combustion Institute, Pittsburgh, 1990.

18. Williams, A., Woolley, R., and Lawes, M., "The Formation of NO_x in Surface Burners," Combustion and Flame 89: 157-166 (1992).

19. Incropera, F.P., and DeWitt, D.P., Fundamentals of Heat and Mass Transfer. John Wiley & Sons. 1985.

20. Nguyen, H.L., Bittker, D.A., and Niedzwiecki, R.W., "Investigation of Low NO_x Staged Combustor Concept in High-Speed Civil Transport Engines", AIAA paper no. AIAA-89-2942, 1989.

21. Sathe, S.B., Kulkarni, M.R., Peck, R.E., and Tong, T.W., *Twenty-Third Symposium (International) on Combustion.* The Combustion Institute meeting, Menlo Park, CA, 18-19 October, 1993.